

AD-A158 949

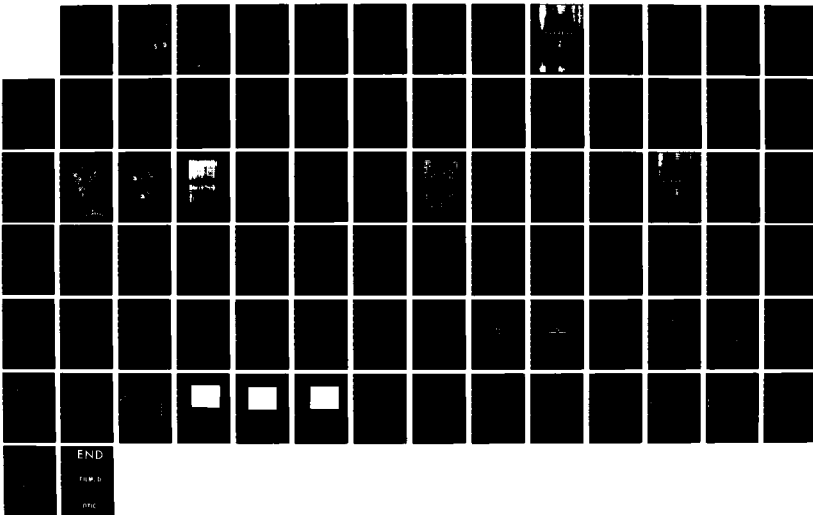
SURFACE PRODUCTION OF NEGATIVE HYDROGEN IONS(U) STEVENS 1/1  
INST OF TECH HOBOKEN NJ DEPT OF PHYSICS AND ENGINEERING  
PHYSICS M SEIDL 18 JUL 85 AFOSR-TR-85-0726

UNCLASSIFIED

AFOSR-83-0230

F/G 20/8

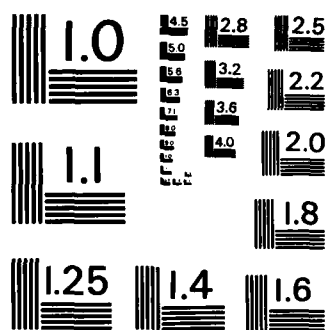
NL



END

1000

000



MICROCOPY RESOLUTION TEST CHART  
NATIONAL BUREAU OF STANDARDS - 1963 - A

**Unclassified**

SECURITY CLASSIFICATION OF THIS PAGE (When Data Entered)

AD-A158 949

REPORT DOCUMENTATION PAGE		READ INSTRUCTIONS BEFORE COMPLETING FORM
1. REPORT NUMBER <b>AFOSR-TR-85-0726</b>	2. GOVT ACCESSION NO. <b>AD-A158 949</b>	3. RECIPIENT'S CATALOG NUMBER
4. TITLE (and Subtitle) Surface Production of Negative Hydrogen Ions -	5. TYPE OF REPORT & PERIOD COVERED Annual Scientific Report (June 1, 1984 to May 31, 1985)	
AUTHOR(s) Milos, Seidl	6. PERFORMING ORG. REPORT NUMBER	
PERFORMING ORGANIZATION NAME AND ADDRESS Department of Physics & Engineering Physics Stevens Institute of Technology Hoboken, NJ 07030	7. CONTRACT OR GRANT NUMBER(s) <b>AFOSR-83-0230</b>	
CONTROLLING OFFICE NAME AND ADDRESS Department of the Air Force Air Force Office of Scientific Research /NP Bolling Air Force Base, DC 20332	10. PROGRAM ELEMENT, PROJECT, TASK AREA & WORK UNIT NUMBERS <b>61102F/2301/A7/</b>	
MONITORING AGENCY NAME & ADDRESS (if different from Controlling Office)	12. REPORT DATE <b>July 18, 1985</b>	
	13. NUMBER OF PAGES <b>7 + 74</b>	
	15. SECURITY CLASS. (of this report) <b>Unclassified</b>	
	15a. DECLASSIFICATION/DOWNGRADING SCHEDULE	
16. DISTRIBUTION STATEMENT (of this Report)  Approved for public release; distribution unlimited.		
17. DISTRIBUTION STATEMENT (of the abstract entered in Block 20, if different from Report)  <b>DTIC ELECTE SEP 10 1985</b>		
18. SUPPLEMENTARY NOTES  <b>S E</b>		
19. KEY WORDS (Continue on reverse side if necessary and identify by block number)  <b>Ion Emission; Atom, Molecule and Ion Impact, Sputtering; Ion Sources</b>		
20. ABSTRACT (Continue on reverse side if necessary and identify by block number)  Measurements of sputtering of adsorbed hydrogen by cesium ion bombardment have been completed. The temperature of the desorbed negative hydrogen ions is about 0.5 percent of the bombarding energy. An experiment for studying bombardment with cesium and hydrogen ions has been constructed. Formation of cesium coverage due to cesium bombardment of a molybdenum target has been studied. Cesium coverage is only weakly dependent on bombardment energy in the range from 100 to 500 eV. This is due to cesium ion implantation.		

DTIC FILE COPY

DD FORM 1 JAN 73 1473 EDITION OF 1 NOV 65 IS OBSOLETE

UNCLASSIFIED

SECURITY CLASSIFICATION OF THIS PAGE (When Data Entered)

### Table of Contents

	Page
1. Research Objectives	1
2. Status of Research	1
2.1. Sputtering of Negative Hydrogen Ions by Cesium Ion Bombardment	1
2.2. Cesium Coverage of Targets Due to Cesium Ion Bombardment	2
2.3 Detector of Hydrogen Atoms	3
2.4. Bombardment of the Target with Hydrogen and Cesium Ions	3
3. List of Publications	4
4. Papers Presented at Meetings	4
5. List of Professional Personnel	5
6. Appendix 1: Stevens Report PSPL 8503 J. Lopes, J. A. Greer, M. Seidl, Sputtering of Adsorbed Hydrogen by Cesium Ion Bombardment.	
7. Appendix 2: Stevens Report PSPL 8502 G. S. Tompa, W. E. Carr, M. Seidl, Cesium Coverage on Molybdenum Due to Cesium Ion Bombardment.	

Accession For	
NTIS GRA&I	<input checked="" type="checkbox"/>
DTIC TAB	<input type="checkbox"/>
Unannounced	<input type="checkbox"/>
Justification	
By _____	
Distribution/	
Availability Codes	
Dist	Avail and/or Special
A-1	

AIR FORCE OFFICE OF SCIENTIFIC RESEARCH LABORATORY  
NOTICE OF FEDERAL INFORMATION PROCESSING ACT REQUEST  
This document contains neither recommendations nor conclusions of the  
Air Force Office of Scientific Research Laboratory. It has been reproduced  
as furnished by the requester. It is the responsibility of the requester  
to ensure that it complies with all applicable laws and regulations.  
DISTRIBUTION STATEMENT A: APPROVED FOR PUBLIC RELEASE  
MATTHEWS, J.  
Chief, Technical Information Division



## 1. Research Objectives

This research consists of experimental and theoretical studies of processes that lead to the production of negative hydrogen ions on solid surfaces. The ultimate goal of the research is to develop quantitative models that would describe surface production of negative hydrogen ions in reasonable agreement with experimental observations. These models should make it possible to assess the effectiveness and limitations of surface production of negative hydrogen ions in various types of ion sources considered for exoatmospheric applications. The research will also contribute to understanding of some basic surface physics problems such as adsorption, atomic scattering, desorption mechanisms and electron transfer in atom-metal interaction.

The stated goal for the past year has been to conclude experiments on production of  $H^-$  ions by sputtering adsorbed hydrogen with cesium ion bombardment and to start studying simultaneous bombardment of targets with cesium and hydrogen ions.

## 2. Status of Research

### 2.1. Sputtering of Negative Hydrogen Ions by Cesium Ion Bombardment.

We have concluded detailed studies of negative particle production due to cesium ion bombardment of a molybdenum target partially covered with cesium and hydrogen. The results are presented in a Stevens Report [1] attached to this report as Appendix 1. Only three particle species are produced:  $H^-$  and  $Mo^-$  ions and electrons. The negative hydrogen ions constitute typically 55 percent of all sputtered charged particles. Their angular distribution can be approximated by a gaussian distribution with an angular half-width spread

of 3 degrees. The H<sup>-</sup> ions are born with a Maxwellian distribution in parallel energies. The temperature of this distribution is very low, between 0.3 to 0.5 percent of bombarding energy (ranging from 150 to 950 volts). The secondary electrons constitute about 30% of the total beam. The temperature of the electron distribution is extremely low, about 0.1 electron volts. The effect of surface roughness of the target on the angular spread of the sputtered H<sup>-</sup> ions and electrons is negligible up to surface roughness of tens of micrometers. The above temperatures correspond to maximum hydrogen and cesium coverage. Patch formation occurring at lower coverages makes the temperature larger. This effect is especially important at low bombarding energies where ion temperature due to incomplete coverage may dominate. At complete coverage the observed H<sup>-</sup> ion distribution is consistent with a desorption model based on elastic binary collisions between Cs<sup>+</sup> ions and hydrogen atoms.

## 2.2. Cesium Coverage of Targets Due to Cesium Ion Bombardment.

Interaction of cesium ions with metal surfaces has been studied in a UHV system the construction of which had been supported by a DOD instrumentation grant (AFOSR-83-0316). This part of the research is also supported by a DOE grant. We have studied cesium coverage of a molybdenum surface bombarded with a cesium ion beam in the energy range of 100 to 900 eV. The cesium ions are produced in a solid state source developed at Stevens several years ago. Results of this work have been summarized in a Stevens Report [2] attached as Appendix 2.

In contrast to conventional wisdom, a steady state regime develops in which cesium coverage depends only weakly on bombarding energy. Theoretical

considerations indicate that this effect is due to cesium ion implantation which changes the upper layers of the original target into a composite material containing about 50 percent cesium atoms. Cesium implantation is the dominant effect whenever the atomic mass of the target is smaller than the atomic mass of cesium. These results may lead to the development of more efficient targets.

#### 2.3 Detector of Hydrogen Atoms.

A commercially available thick film semiconductor material of 1 x 1 mm area has been tested for detection of atomic hydrogen [3]. In accordance with published data the detector is selective for atomic hydrogen and insensitive to molecular hydrogen. Its disadvantage is easy saturation with hydrogen occurring at higher hydrogen fluxes. It is, however, felt that the detector will be suitable to measure sputtering yields of hydrogen atoms. These results, in combination with H<sup>-</sup> ion yield measurements, will make it possible to measure the electron transfer probability in the sputtering process.

#### 2.4. Bombardment of the Target with Hydrogen and Cesium Ions.

In this experiment the target will be bombarded with cesium and hydrogen ions. This is the standard operational regime of surface conversion sources. However, the ratio of the two ion fluxes hitting the target has never been measured in these sources.

We have designed and built an experimental diode in which the ratio of the two ion fluxes will be measured and controlled. In this experiment

we shall investigate hydrogen ion implantation in the 100 eV energy range which has not been done before. We shall study the effect of hydrogen implantation on H<sup>-</sup> yield and evaluate the relative importance of cesium and hydrogen sputterings.

### 3. List of Publications

- 1) J. L. Lopes, J. A. Greer, M. Seidl, Sputtering of Adsorbed Hydrogen By Cesium Ion Bombardment. Stevens Report PSPL 8530 (July 85). To be submitted to Journal of Applied Physics.
- 2) G. S. Tompa, W. E. Carr, M. Seidl, Cesium Coverage on Molybdenum Due to Cesium Ion Bombardment. Stevens Report PSPL 8502 (July 85). To be submitted to Journal of Applied Physics.
- 3) R. P. Szwerc, The Detection of Atomic Hydrogen. Senior Thesis, Stevens Report PSPL 8501.

### 4. Papers Presented at Meetings

- 1) G. S. Tompa, W. E. Carr, M. Seidl, Cesium coverage in the negative hydrogen converter sources. Division of Plasma Physics APS Annual Meeting, Boston, Oct. 1984 (Paper 5x8).
- 2) J. L. Lopes, M. Seidl, Energy distribution of negative hydrogen ions sputtered by cesium bombardment. APS Division of Plasma Physics Annual Meeting, Boston, Oct. 1984 (Paper 5x9).

**5. List of Professional Personnel**

**Faculty:**      **Milos Seidl, Professor of Physics**  
                     **Wayne Carr, Associate Professor of Phys8cs**

**Graduate Doctoral Students:**

**Gary Tompa**  
**Joseph Lopes**  
**Andrew Souzis**

**Master's Student:**    **Richard Szwerc**

**Technician:**        **George Wohlrab**

CESIUM COVERAGE ON MOLYBDENUM  
DUE TO CESIUM ION BOMBARDMENT

G. S. Tompa, W. E. Carr, M. Seidl

Department of Physics and Engineering Physics

PSPL8502

**S T E V E N S**  
**INSTITUTE OF TECHNOLOGY**



CASTLE POINT • HOBOKEN, NEW JERSEY 07030

CESIUM COVERAGE ON MOLYBDENUM  
DUE TO CESIUM ION BOMBARDMENT

G. S. Tompa, W. E. Carr, M. Seidl

Department of Physics and Engineering Physics

PSPL8502

## CESIUM COVERAGE ON MOLYBDENUM DUE TO CESIUM ION BOMBARDMENT

G. S. Tompa, W. E. Carr, M. Seidl

### ABSTRACT

Formation of cesium coverage due to cesium ion bombardment of a molybdenum target is studied. The cesium ions are extracted from a zeolite source, accelerated and focused onto the molybdenum surface, and the change in the workfunction is measured as a function of doseage. The end point workfunction change is not strongly dependent on energy, in the range of 150eV. to 900eV. the workfunction shift is observed to decrease by 0.4eV.. This corresponds to a coverage change of .20, starting from a maximum of ~.62 at 150eV.. The coverage is interpreted from the change in workfunction. The steady state coverage cannot be accounted for by a simple sticking and sputtering relationship, but must at least include a contribution due to cesium implantation. Other analytic techniques are used to provide supplemental infomation.

### INTRODUCTION

In past years the production of  $H^-$  beams has become of importance to the fusion program as well as military applications. An important method of production is surface conversion. In surface conversion  $H^-$  sources the converter surface is immersed in a cesium-hydrogen plasma. Cesium coverage reduces the workfunction of the converter, thereby increasing the yield of  $H^-$  from the surface. There exists an optimum coverage at which the workfunction is a minimum and hence the yield is a maximum<sup>1,2</sup>. Unfortunately in working converter sources the surface coverage is not well known, precipitating this experiment<sup>3</sup>. Within the plasma the mean free path

of neutral Cs is small, implying that the majority of the surface coverage is due to  $\text{Cs}^+$  bombardment as opposed to a neutral contribution. The converter typically is biased at a few hundred volts negative with respect to the plasma potential. The purpose of this experiment was to investigate an aspect of converter sources that is not well known, the build up and maintenance of an equilibrium cesium coverage due to cesium ion bombardment.

The Cs surface coverage formation process is investigated in the 150eV. to 900eV. energy range, which is relevant to surface converter sources. In our experimental system the surface coverage may be determined by AES, ISS, and retarding field electron beam workfunction shift measurements. SIMS may be used to determine surface and subsurface changes. Polycrystalline molybdenum is bombarded with positive cesium ions. Molybdenum was chosen as the first material to investigate since it gives the best yields of  $\text{H}^-$  to date. A zeolite cesium ion source provides the ions to bombard the target. The experimental data are obtained on sputter cleaned targets in an ultrahigh vacuum chamber. The workfunction is monitored as a function of cesium ion dosage at a given energy until steady state is reached. The dosage is determined by monitoring the beam current to the target. The workfunction change is seen to decrease with increasing bombarding energy implying a decreasing coverage.

The surface Cs coverage is primarily governed by two processes, the retention of incoming  $\text{Cs}^+$  and the sputtering of surface particles. The initial surface sticking coefficient is measured as a function of bombarding energy, by examining the initial rate of coverage formation. The coefficient is found to drop significantly with increasing energy, suggesting that the retention coefficient is not simply a sticking coefficient. Simple theories neglecting the contribution of implanted cesium to the final coverage are shown to be inconsistent with observed coverages. A full theory must take into account implantation, which depends on the masses and energies involved.

## EXPERIMENTAL APPARATUS

The general surface analytical system setup is depicted in figure 1. The experimental test chamber is a Varian 2000 series stainless steel bell. All ports are of the "conflat" type providing all metal seals. The main pumping is provided by a Perkin-Elmer TNBX-300 ion pumping system including titanium sublimators and cryopanels. The chamber pressure is monitored with a nude ionization guage controlled by a Perkin-Elmer DGC III ionization guage controller. Several observation windows are mounted on the chamber including one large main observation window. The chamber and all appendages are bakeable in excess of 150 degrees centigrade. Typical post bakeout pressures of 1E-8 pascal are standard. All inert gas ion guns are differentially pumped. Provision is made for admitting any gas into the chamber at any pressure, in particular for backfilling the chamber with nitrogen or operating at a fixed flux of a given gas.

The sample, shown in figure 2, is supported on a base which mounts onto an internal carousel, and may be inserted or withdrawn from vacuum through a port. It is isolated and biasable through internally mating shielded cable. Two additional leads are presently supporting a cesium shield which was found neccessary to prevent leakage currents due to the formation of cesium coatings on insulators in the target region. This arrangement takes advantage of the sputter cleaning capabilities of the Perkin-Elmer sputter ion gun model 04-303 which is capable of cleaning the sample surface. The sample is placed at a convenient angle for the analytic tools. The sample area is greatly reduced from previous designs, easing alignment and assuring a uniform coverage by the cesium ion beam.

The sample is transferred via a long metal rod threaded at one end and attached to a rotary feedthrough at the other. The sample threads onto the rod and is pushed onto the carousel where spring clips hold it in place and push pin connectors make electrical contact. The rod is then unthreaded and withdrawn. The docking port consists of an alignment adapter nipple and a five-way cross through

- 19.) P. D. Townsend, J. C. Kelly, and N. E. W. Hartley, Ion Implantation, Sputtering, and their Applications, Academic Press (1976) page 32.
- 20.) Ubai A. Arifov, Interaction of Atomic Particles With a Solid Surface, Consultations Bureau New York-London 1969
- 21.) J. Bohdansky, Nucl. Instr. Meth. in Phys. Res. **B2** (1984) 587

## REFERENCES

- 1.) J. R. Hiskes, *Journal de Physique C7 N7 TOME 40* (1979)
- 2.) M. Seidl and Andrew Nason Pargellis, *Physical Review B V26 N1* (1982)
- 3.) K. W. Ehlers and K. N. Leung, Production and Neutralization of Negative Ions and Beams, 3rd International Symposium, Brookhaven, (1983), pages 227-236
- 4.) J. D. Allen, Jr., J. Preston Wolfe and G. K. Schweitzer, *Intl. J. Mass Spec. Ion Phys.*, **8**, 81, (1972)
- 5.) J. D. Allen, Jr., J. D. Durham, G. K. Schweitzer and W. E. Deeds, *J. Electron Spectr. Related Phenomena* **8**, 395 (1976)
- 6.) G. Carter, J. S. Colligon, Ion Bombardment of Solids, American Elsevier Publishing Company (1968) pg. 65
- 7.) L. W. Swanson, R. W. Strayer, *J. Chem. Phys.* **V48 N6** (1968)
- 8.) Ming L. YU, *Phys. Rev. Lett.*, **V40 N9** (1978)
- 9.) U. V. Azizov, B. E. Egamberdiev, and A. Kashetov *Sov. Phys. Tech. Phys.* **28(1)** (1983)
- 10.) L. E. Davis, et. al., Handbook of Auger Electron Spectroscopy, Physical Electronics Industries, Inc., (1976)
- 11.) L. H. Taylor, *Surface Science* **2** (1964) 188-199
- 12.) T. J. Lee and R. E. Stickney, *Surface Science* **32** (1972) 100-118
- 13.) P. W. van Amersfoort, J. J. C. Geerlings, L. F. TZ. Kwakman, E. H. A. Granneman and J. Los paper submitted to *J. Appl. Phys.* (1985)
- 14.) P. W. van Amersfoort, Ying Chun Tong and E. H. A. Granneman, paper submitted to *J. Appl. Phys.* (1985)
- 15.) John Bradshaw Taylor and Irving Langmuir, *The Physical Review*, **V44**, N6 (1933)
- 16.) P. Akhter and J. A. Venables, *Surface Science* **103** (1981) 301-314
- 17.) D. L. Fehrs and R. E. Stickney, *Surface Science* **24** (1971) 309-331
- 18.) J. Lindhard, M. Schariff, and H. E. Schiott, *Kgl. Danske Selsk. Matt-Fys. Medd.* **33** No. 14 (1963)

#### ACKNOWLEDGMENTS

Special thanks goes to George Wohlrab whose machining capabilities and general assistance in keeping the experiment running are greatly appreciated and to Gunther Wurth who also machined many of the system components. This work was supported Air Force Office of Scientific Research contract grant 5-27739 and Department of Energy contract grant 5-27455.

is not strongly energy dependent, and this is qualatively true in the experiment where the coverage change is .20 for nearly an order of magnitude change in voltage. This model is only a crude first step and we do not expect it to be quantitatively correct. We plan in the future to use more sophisticated sputtering codes in an attempt to get an accurate model.

An important parameter is the cesium sputter coefficient. In steady state the cesium ion flux to the surface must equal the flux of cesium leaving the surface. This relates the coverage to the sputter coefficient:  $\theta_E = 1/Y$ , hence the energy dependence of  $Y$  determines the energy dependence of coverage. Arifov<sup>20</sup> gives a sputter yield of cesium ions of ~.60 at a cesium ion bombarding energy of 150eV., decreasing at higher or lower energies. A few percent of the sputter yield is due to the essentially elastic multiple scattering of cesium from the molybdenum surface. Using Arifov's<sup>20</sup> results we see that at high energies  $\theta_E$  would increase, which is in disagreement with our results. Arifov's<sup>20</sup> measurements include neither the neutral yields nor sputtered target material, ionized or neutral. Amersfoort et. al.<sup>13,14</sup> using Bohdansky's<sup>21</sup> theoretical formulation derived a value which is unity for engergies of  $>100$ eV. for cesium, and increases with energy. These are in qualitative agreement with our results.

Presently we are repeating and refinig our experimental results on molybdenum. This includes repeating the workfunction measurments down to zero deposition energy to further understand the interplay of surface migration and the onset of implantation, quantifying the auger spectra and performing ion scattering spectroscopy. In addition we will perform depth profiling in an attempt to measure the cesium implantation profile. We will also continue to refine the theoretical understanding of the role of implantation in coverage. We also plan to study other targets. In particular we will try beryllium and tungsten to study the effect of target mass.

where  $\Delta n_c$  is contribution to the cesium concentration while it is at depth  $x$ ,  $r$  = the average depth (projected range) and  $\rho$  = the width of the gaussian profile (straggling).

The steady state cesium concentration at a depth  $x$  beneath the surface is the sum of all the implanted ions while that layer of material was a distance greater than  $x$  from the surface:

$$n_c(x) = \int \Delta n_c(x) = (n_c n_* / 2.5 n_m) \int_u^\infty \exp(-v^2) dv \quad (7)$$

where  $u = (x-r)/\rho$ , and (3) through (5) have been substituted to obtain this form. For the concentration just below the surface, we evaluate at  $x = 0$  to obtain;

$$n_m = C n_* \quad (8)$$

where  $C$  is a numerical constant which depends on the depth and spread of the implanted particles. It is relatively insensitive to the material parameters; typically  $C$  varies from 0.65 to 0.77. This model shows that the bulk molybdenum and cesium concentrations near the surface are weakly dependent on the incident energy through the implantation depth and spread.

It should be noted that the surface coverage is not the same as the concentration just below the surface. The surface is preferentially sputtered, i.e., the surface adjusts so that the sputtered fluxes equal the concentrations in the bulk, which is necessary for steady state to exist.

According to this picture a low energy ( $<200$ eV.) cesium beam is essentially deposited on the surface, so the initial coverage is relatively large. At higher energies the cesium is implanted several layers, and relatively few are on the surface initially. After sputtering many layers away steady state is reached, with a significantly larger coverage. According to (8) the final value

instant of time the incident cesium is implanted and some of the surface is sputtered away, exposing previously implanted cesium. There are computer codes which should be able to model the dynamic process, and we plan to study this in the future.

When the surface is exposed to the cesium beam for a long enough time it ceases to change. Under these steady state conditions we can derive an analytical result. Since there is no net cesium accumulation, we have that the sputtered flux of cesium  $\phi_c$  equals the incident flux  $\phi_{in}$ ;

$$\phi_c = \phi_{in} \quad (3)$$

Here incident flux is the net flux, i.e. beam flux minus reflected flux. Once there is a buildup of cesium on the surface the reflection of incident cesium ions will increase. The material just under the surface has a fixed concentration of cesium,  $n_c$ , and molybdenum,  $n_m$ . The ratio of sputtered fluxes must therefore be given by;

$$\phi_c / \phi_m = n_c / n_m \quad (4)$$

where  $\phi_m$  is the sputtered molybdenum flux. There is a surface erosion speed given by;

$$V = \phi_{out} / n_* = \phi_m / n_* \quad (5)$$

This is the net flux leaving the surface normalized to the total particle density in the solid,  $n_*$ . But by (3) the net cesium flux is zero, therefore  $\phi_{out} = \phi_m$ .

The instantaneous implantation profile is gaussian, and may be written as<sup>19</sup>;

$$\Delta n_c(x) = \frac{\phi_{in} \Delta x}{2.5 \rho V} \exp\left[-\frac{(x-r)^2}{\rho^2}\right] \quad (6)$$

On converters in a discharge, cesium may be assumed to be spread uniformly on the converter surface due to the discharge, hence migration is not important for converters.

We believe that implantation is necessary to describe these results. Since cesium has a greater mass than molybdenum it is scattered in the forward direction only, the maximum angle being  $-46.2^\circ$ . This implies that incident cesium ions penetrate the surface. Assuming implantation, the initial workfunction will be that of molybdenum with a small amount of surface cesium. As time goes on molybdenum is sputtered away and the implanted cesium is exposed and also sputtered away. This leads to a final steady state cesium coverage.

We have calculated the implantation depth profile of cesium in molybdenum using a random collision model. We treat the solid as a random collection of spheres with size equal to that of a molybdenum ion, with the appropriate interparticle spacing. We then follow a cesium ion through a series of random collisions until the cesium energy is below the typical binding energy or the ion is reflected. Figure 8 shows histograms of  $1E+4$  particles for low and high incident energies. Since the thickness of a layer is a few Å, particles at depths of less than this are on the surface and those at larger depths are below the surface. Low energy implantation gives a large fraction on the surface, while at higher energy the fraction on the surface decreases. This is in qualitative agreement with the energy dependence of the initial sticking coefficient that is observed experimentally. We can compare the implantation depth scale with the LSS<sup>18</sup> theory of implantation. This gives a relation between incident energy and range for low energy (less than 10 KeV.) cesium on molybdenum given by;  $D = 11.4 A E^{2/3}$  ( $E$  in KeV.) which is in reasonable agreement with our values.

The above results give a depth profile assuming that there is no surface erosion by sputtering. In the experimental situation both cesium and molybdenum are sputtered. Thus at each

TABLE 1

ION BEAM ENERGY	$\Delta\phi$ eV EQUIL	$\theta_E$	$\alpha$	$\gamma_1$	$\gamma_2$
150	2.65	62%	.65	.39	1.04
200	2.58	55%	.52	.42	.94
250	2.55	53%	.35	.31	.66
350	2.50	52%	.25	.23	.47
450	2.50	52%	.06	.05	.11
500	2.45	49%	.03	.03	.06
750	2.30	42%	.02	.03	.05
900	2.25	41%	.01	.02	.03

We believe the model given by (1) does not adequately describe our measurements because it is too simple. One of the effects not included is cesium surface migration. For tungsten Taylor and Langmuir<sup>15</sup> give a site lifetime of 1.5E-5 seconds at 300° K and a site to site distance of 2.6E-8 cm.. Assuming that similar values hold for molybdenum an average straight line maximum velocity of ~1mm/minute may be estimated if one assumes the sites in the line of travel are vacant. Akhter and Venables<sup>16</sup> have also examined the surface migration obtaining results similar to Taylor and Langmuir<sup>15</sup>. At low bombarding energies, <20eV., workfunction shifts were not easily repeatable. Readings could be observed to change during the measurement period, which is ~1 minute. Fehrs and Stickney<sup>17</sup> had similar problems on tungsten which they attributed to cesium migration. This problem arises when a large area on the target is examined compared to the area of uniform coverage and/or measurements are made on a time scale comparable to or greater than the time for the coverage to substantially change due to migration. At higher energies there was no evidence of migration affecting the workfunction shift measurements.

et. al.<sup>13,14</sup>). Our relation gives a lower  $\theta_E$  than their expression. Amersfoort et. al.<sup>13,14</sup> have a discussion of cesium on tungsten, where they conclude that a coverage greater than 26% of a monolayer cannot be maintained if the cesium component is highly ionized. Our measurements show much higher coverage, see fig. 4b, for measured end-point coverage versus energy for cesium on molybdenum.

The sticking coefficient on a clean surface is obtained by evaluating the initial rate of change of coverage. Evaluating (1) at  $\theta = 0$ , we have that;

$$(\alpha_0/\phi)(d\theta/dt) = \alpha \text{ at } \theta = 0 \quad (2)$$

Note that this is valid for both forms of (1). Using measured values of incident flux and initial slope of coverage versus time in (2), we obtain initial sticking coefficient as a function of energy shown in figure 7. The initial sticking coefficient decreases sharply with increasing energy until ~350 volts where it levels off at very low values. At very low energy the sticking coefficient approaches 1. Under the reasonable assumption that the sticking coefficient will not increase with increasing cesium coverage, figure 7 gives an upper bound to  $\alpha$  for finite coverage.

We can estimate the yields using measured quantities along with the values in figure 7. Table 1 contains the sputtering yields as well other relevant data.  $\gamma_1$  is determined by our formulation and  $\gamma_2$  by Amersfoort's<sup>13,14</sup> equivalent relation. The low values of  $\alpha$  at higher energies combined with the equilibrium coverages observed result in unrealistically low values of  $\gamma$ .  $\Delta\phi$  is the work function shift.

at the workfunction station. After an initial shift in the first two minutes the workfunction is seen to be essentially constant for approximately one hour. This type of behavior is also observed for targets coated with cesium or exposed to hydrogen gas at a pressure two orders greater than the background pressure after cleaning. (Of course the starting points of the curves are different from the clean surface.) It would seem from the figure that a rapid initial shift of .1eV. may in general add to the error of our measurements. Contamination is a problem but is not believed to have a significant effect on results.

#### DISCUSSION

We first attempt to interpret the results with a formula we have used in the past, given by;

$$\sigma_0 d\theta/dt = \alpha\phi(1-\theta) - \gamma\theta \quad (1)$$

where  $\sigma_0$  = the number defining a monolayer  
 $\theta$  = the coverage  
 $\alpha$  = the sticking coefficient  
 $\gamma$  = the sputtering coefficient  
 $\phi$  = the flux of cesium ions to the surface  
 $d\theta/dt$  = rate of change of coverage

This formulation assumes that all cesium that stays on the metal sticks to the surface, and neglects the evaporation of cesium from the surface. The neglect of evaporation is reasonable at an operating temperature of 300° K<sup>11,12</sup>. Amersfoort et. al.<sup>13,14</sup> has a similar formulation, the difference being that they do not include the (1-θ) factor in their relation. This factor accounts for the fact that an incoming cesium will not stick at a site already occupied by a cesium atom.

The end-point coverage is determined by the right hand side of (1), given by,  $\theta_E = \alpha/(\alpha+\gamma)$  (or  $\alpha/\gamma$  according to Amersfoort

initial slopes are seen to decrease in magnitude as the energy is increased. The end-point coverages as a function of incident energy are shown in figure 4b. The optimum coverage for the production of H<sup>-</sup> is approached at the lowest energy examined. The workfunction minimum occurs at a surface coverage of ~1.9E14 atoms/cm<sup>2</sup><sup>7</sup>. The equilibrium state is typically reached after ion dosages exceeding 1E16 ions/cm<sup>2</sup>. Converters may be assumed to work at currents densities exceeding 100mA/cm<sup>2</sup>, corresponding to a flux of 6.25E17 particle/cm<sup>2</sup>-sec, thus it is safe to assume that a converter is operating at steady state coverage in less than a tenth of a second.

Auger spectra are also used for determining the coverage. Figure 5 shows the unprocessed peak to peak signal intensities as a function of bombarding energies. Unfortunately the time needed to obtain this data was long compared with the time to accumulate significant contamination onto the target. The cesium coverage is seen to monotonically decrease with increasing energy. The oxygen is the chief contaminant due to the presence of CO and H<sub>2</sub>O as background gasses in the vacuum system. The carbon although observable was not monitored. It should be pointed out that in auger electron spectroscopy oxygen has a sensitivity ~3 times greater than both carbon and cesium. The sensitivity of molybdenum is ~2 times that of cesium. Hydrogen, of course, does not have an Auger spectrum<sup>10</sup>. The molybenum signals predominate throughout the range examined, but diminish at both low energies and high energies. At low energy cesium becomes the major element at the surface. At high energies the time needed to reach equilibrium is longer and hence the contamination peak begins to have a larger effect on the measured signals. In the future ion scattering spectroscopy will also be used in determining the equilibrium coverage.

In order to determine surface stability and the importance of contaminants we monitored the workfunction of a surface versus time. Figure 6 shows the time dependence of the work function of a clean sample. A certain amount of delay is encountered between cleaning and measuring due to the time taken to reposition the sample

workfunction, also shown in figure 2, is a modified Apex model 4760 electron gun. The standard lens system has been replaced by a simple drift tube. The electron source is a custom fitted tungsten filament. Originally a standard barium oxide cathode was used but this has two drawbacks. First, the cathode is poisoned on exposure to atmosphere once it has been activated, necessitating gun replacement whenever the chamber is opened. Second, the tungsten filament is more immune to adsorbate induced shifts in the cathode work function than is barium oxide. It is sometimes possible to reactivate the barium oxide but not in a consistent manner. The electron gun is operated at fixed voltages and the target potential is swept to give retarding field current versus voltage scans.

## RESULTS

In figure 3a are shown typical raw data plots of the workfunction versus the dose. In all cases the workfunction decreases with increasing dosage until it reaches a final, or end-point value. Note also that there is structure in the form of a plateau in each curve. The workfunction of clean polycrystalline molybdenum is taken to be 4.2eV.<sup>7</sup>. The minimum workfunction is downshifted by ~2.6eV. at a coverage of ~.70<sup>7,8,9</sup>. Figure 3b shows the end-point workfunction shift plotted against the cesium beam energy. At 150eV. the workfunction shift is -2.6eV. indicating that the optimum coverage is obtainable by cesium ion bombardment. The workfunction shift is seen to decrease by ~.4eV. as the incident energy varies from 150eV. to 900eV.. For the Mo-Cs surface system a decreasing workfunction shift implies an increasing workfunction. This increase would have substantial effects on converter yields.

The increase in end-point workfunction with increasing beam energy implies a decrease in cesium coverage. The coverage is interpreted from the measured workfunction shifts by comparing to the values of Swanson and Strayer<sup>7</sup>. Figure 4a depicts three processed coverage versus dose plots. In the figure different energy ranges are shown than in figure 3a and the plateaus are again observable. The

energy. Finally a reactive gas "O<sub>2</sub>" may be directed onto the sample to enhance certain emissions.

The cylindrical mirror analyzer "CMA" analytic station is capable of functioning in several modes. In normal operation it is an energy analyzer of Auger electrons. In the retarding mode it may again examine Auger electrons or perform x-ray photoelectron spectroscopy "XPS or ESCA". By reversing polarity in the mirror positive ions may also be examined. In particular a scattered ion energy spectrogram may be recorded "ISS". In general a spectrum as a function of energy for any charged particle emanating from a small fixed area may be obtained. The analyzer is a Perkin-Elmer 15-255GAR double pass angle resolved aperture limited cylindrical mirror. For Auger spectroscopy there is an electron gun coaxial with the cylinder. The Perkin-Elmer 04-303 differential ion gun is used to provide ions for ion scattering spectroscopy. This gun has a high current density and is also used for sputter cleaning of targets.

A cesium ion gun is used to bombard the target, both are depicted in figure 2. The source of cesium is a zeolite pellet fitted in a "Pierce gun" extraction system. An Einzel lens provides further focusing of the beam for extended travel. This lens also controls the final beam size on the target. The beam is next deflected before impinging onto the sample surface. This allows for precise monitoring of the amount of cesium arriving at the surface since neutrals are not deposited, having no optical path to the surface. The yield of electrons at low alkali coverages in this energy range and temperature is not significant<sup>6</sup>. The target is first cleaned by argon ion sputtering. A beam of cesium ions at a given energy then bombards the surface. The surface conditions may be determined by rotating the sample to any of the analytic stations. This allows measurement of surface properties versus dose, with cesium beam energy as a variable parameter. In particular, greatest use has been made of the workfunction measuring station.

The electron diode for measuring shifts in the

which the sample fits. The top of the cross has a window to check the sample in its vacuum environment. A Huntington MS-154 straight through all metal seal valve provides isolation to the chamber. Pressure in the transfer chamber is monitored by a nude ionization guage and a Veeco 1000 controller. High vacuum pumping is provided by a Balzers TPU-040 turbopump backed by a zeolite trapped forepump.

The secondary ion mass spectroscopy "SIMS" instrument consists of two main elements and their support electronics. These are the KRATOS Minibeam II ion gun and the quadupole mass spectrometer. The Minibeam II ion gun has a beam energy of 50eV. to 4 keV.. The gun provides a current varying from 4nA. to 300nA. with a beam diameter varying between 35um. and 100um.. The beam is capable of rastering a 2mm. by 2mm. area on the sample, position on the target is adjustable. The operating gas is typically argon but any noble gas is acceptable. The quadrupole mass spectrometer is the UTI model UTI-100-C modified by Kratos to produce energy filtering of incoming positively or negatively charged particles and block neutrals sputtered from the surface while still retaining the ability to work as a residual gas analyzer. The energy filter is a "Bessel box"<sup>4,5</sup> type arrangement which also blocks on axis neutrals. The mass range is 1 to 300 AMU.. The sweep time is variable from 75ms. to 10min. internally, or may be driven by an external ramp with any period greater than 75ms.. Any portion of the full range may be examined including a single fixed peak. Resolution is 2M at 10% peak height valleys. A channeltron electron multiplier is used for signal detection allowing both pulse counting and analog detection. A gain of 1E+6 is standard.

The SIMS system may operate in the residual gas analysis "RGA" mode with or without sputtering and it may scan the positive or negative 0 to 300 atomic mass unit range. The system is capable of rastering the the sample and gating the signal for more accurate sample profiles. In the raster mode of operation an image of the sample may be obtained. The image may be either an elemental image of the surface or a current to the sample surface image. In both imaging modes the maximum area examined is dependent on the beam

## FIGURE CAPTIONS

FIGURE 1. The general surface analytical system setup

FIGURE 2. The cesium deposition station and the workfunction station are shown in their relation to the sample.

FIGURE 3.a Experimentally obtained workfunction shifts as a function of bombarding ion dosage at energies of 200eV and 350eV.

FIGURE 3.b The equilibrium value of the workfunction shift as a function of bombarding energy.

FIGURE 4.a The coverage on the surface as determined from the workfunction shifts for the bombarding energies of 500eV, 750eV and 900eV.

FIGURE 4.b The equilibrium value of the coverage as a function of bombarding energy.

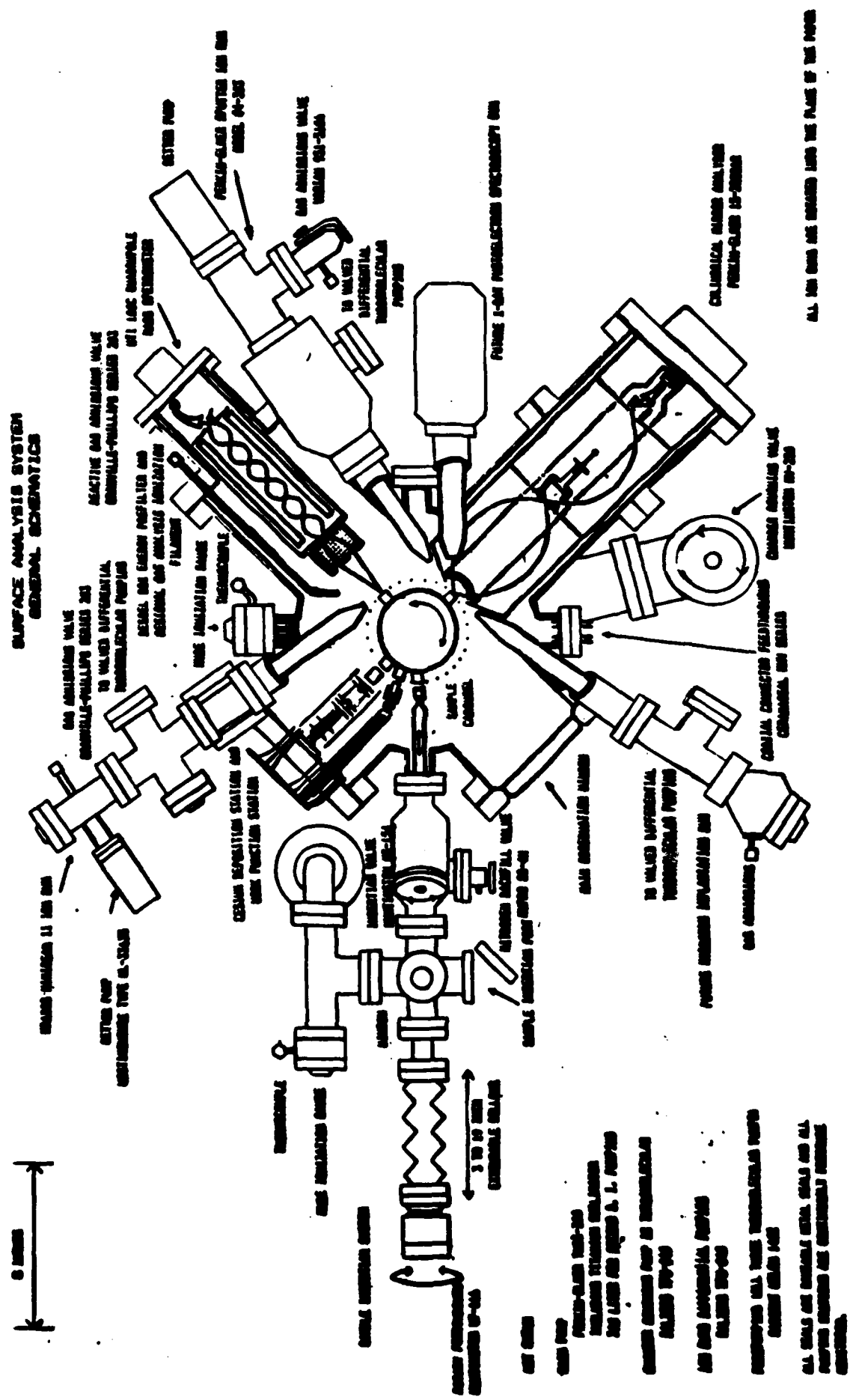
FIGURE 5. Unprocessed auger peak to peak signal intensities as a function of energy.

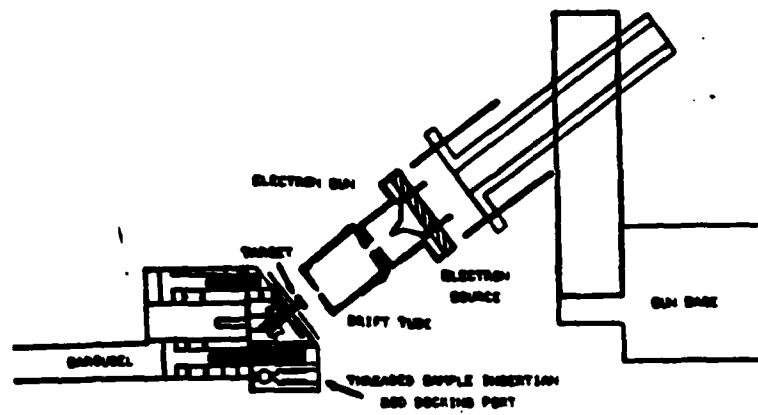
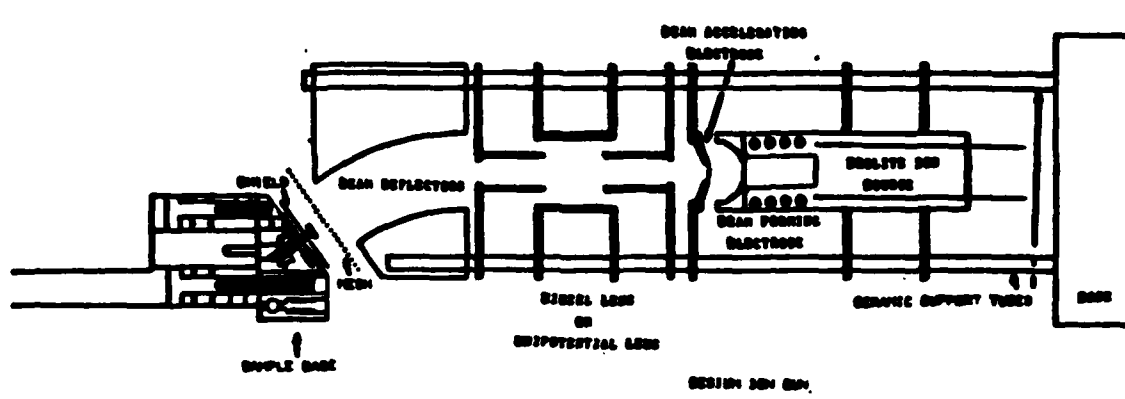
FIGURE 6. The workfunction shift of a clean surface due to background contamination as a function of time.

FIGURE 7. The initial sticking coefficient as a function of energy.

FIGURE 8. Calculated implantation depth profiles of cesium in molybdenum.

FIGURE 1.





**FIGURE 2.**

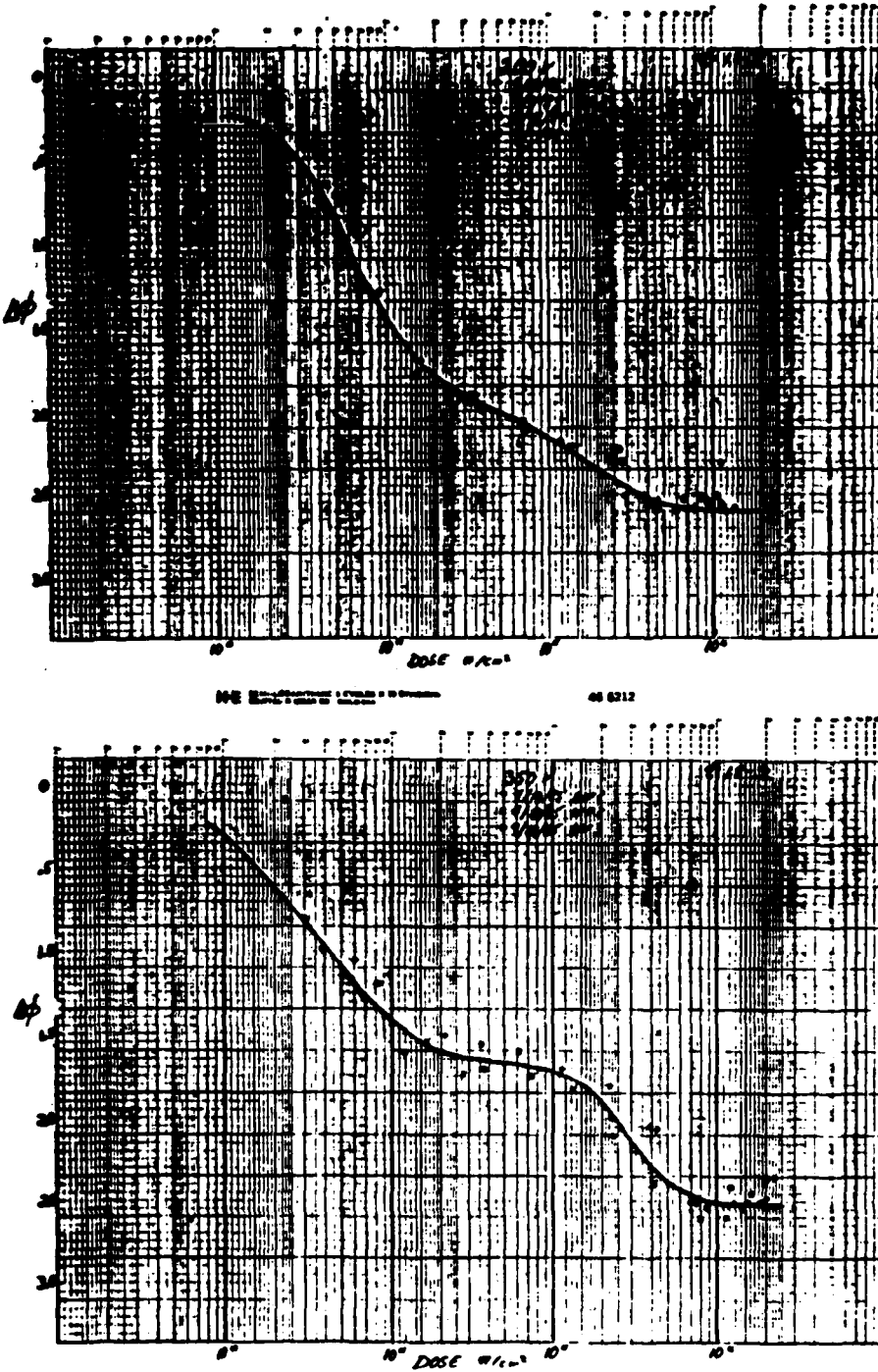


FIGURE 3.a

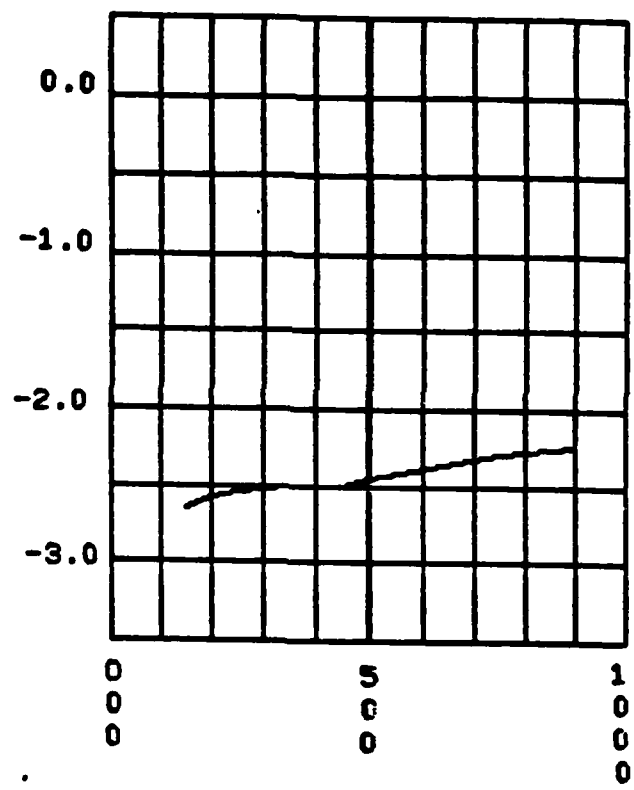
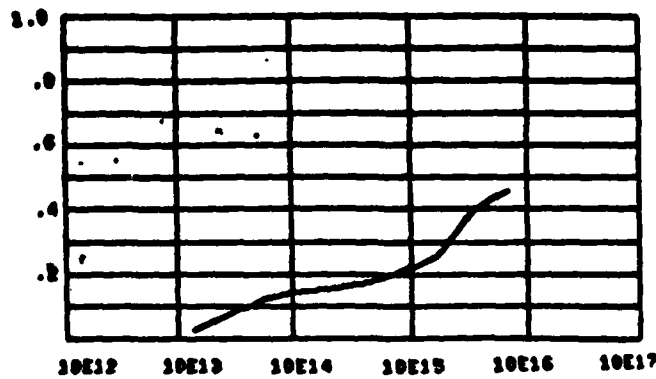
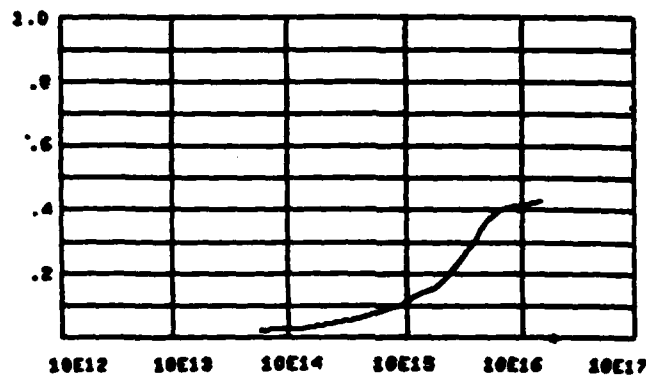


FIGURE 3.b

COVERAGE vs. EDEE90.DAT



COVERAGE vs. EDEE70.DAT



COVERAGE vs. EDEE100.DAT

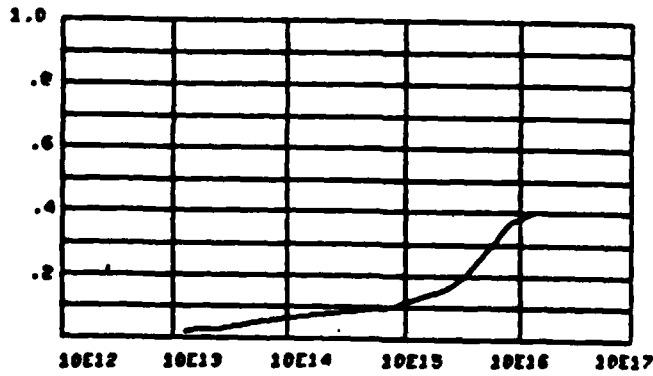


FIGURE 4.a

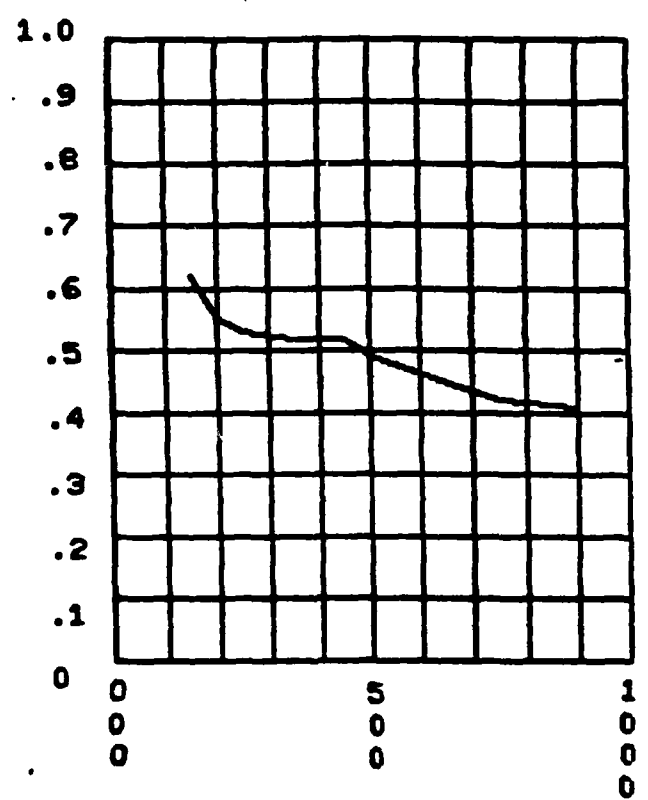


FIGURE 4.b

$\text{K} \cdot \text{E}$  in  $\text{n} \cdot \text{m}$  per centimeter

461510

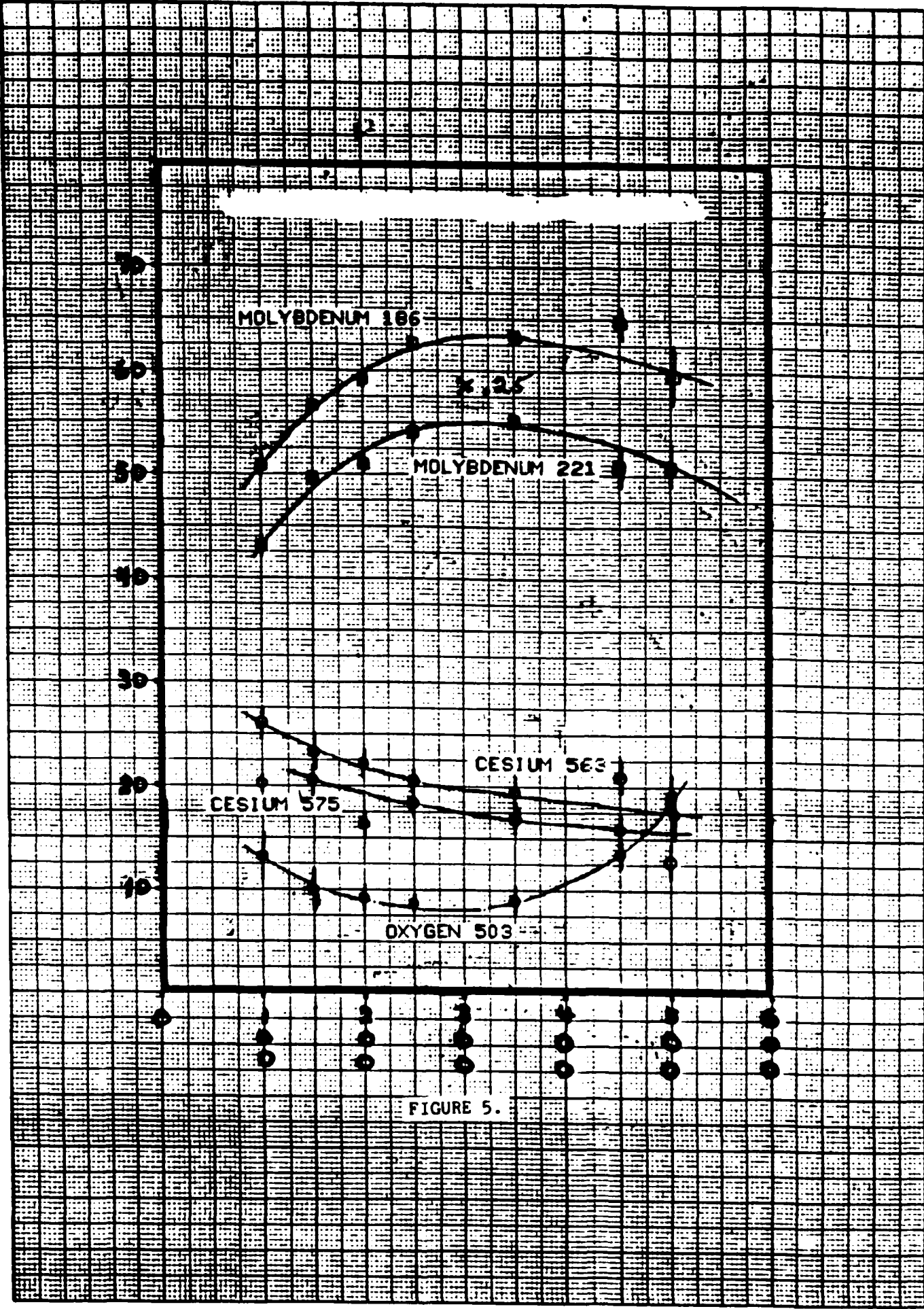
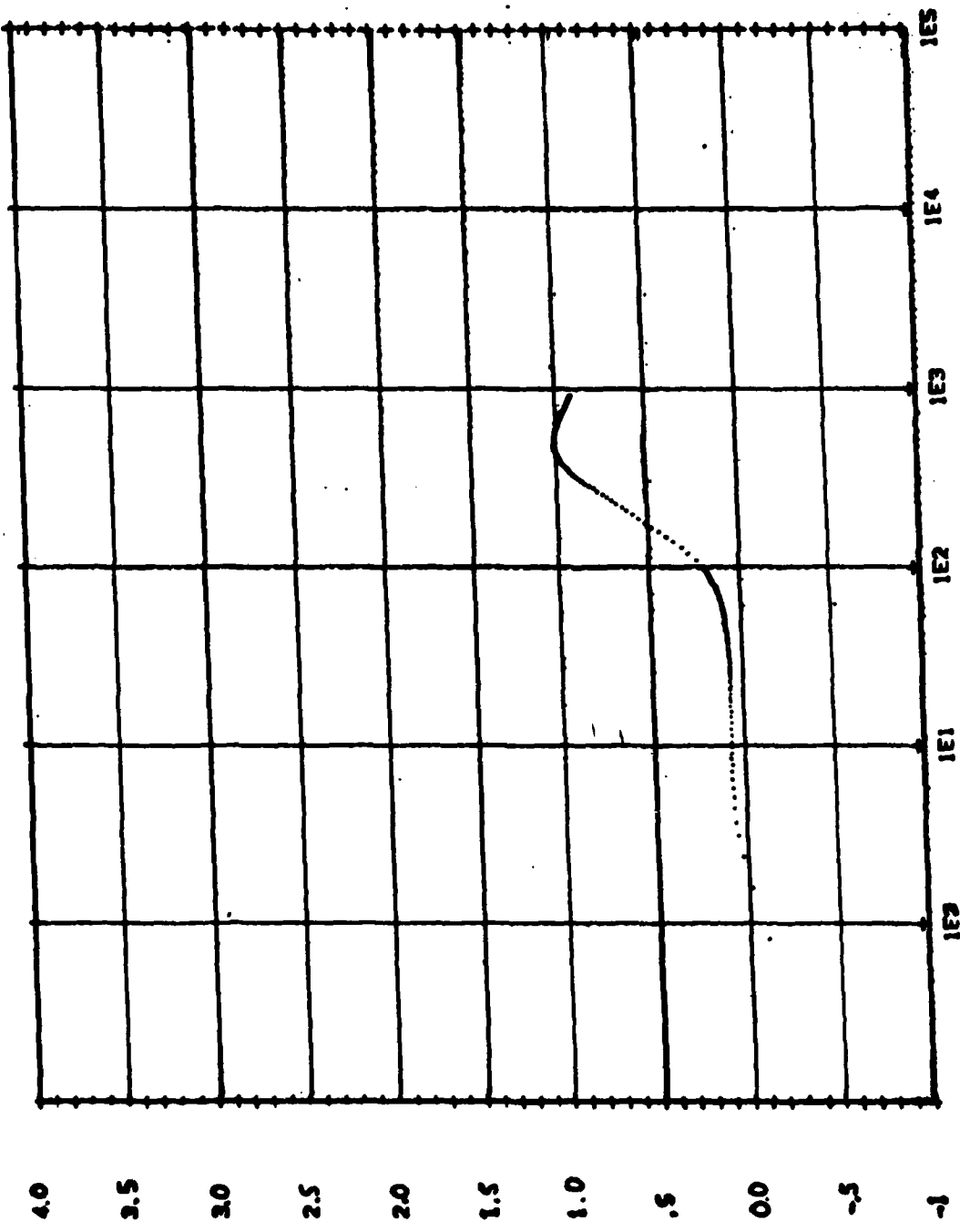


FIGURE 6.



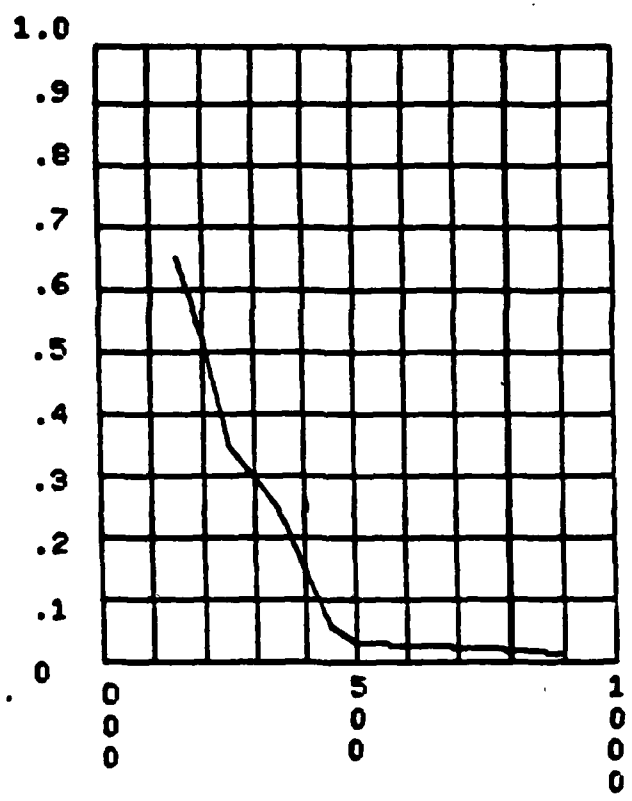


FIGURE 7.

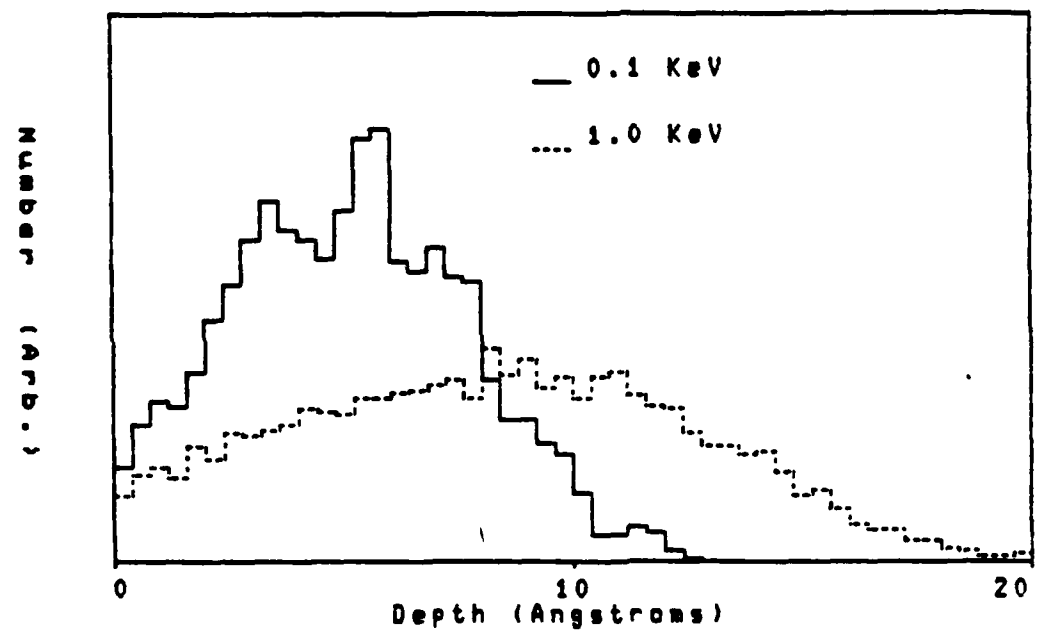


FIGURE 8

Sputtering of Adsorbed Hydrogen

By Cesium Ion Bombardment

J. L. Lopes, J. A. Greer and M. Seidl

Department of Physics and Engineering Physics

PSPL8502

**S T E V E N S**  
INSTITUTE OF TECHNOLOGY



CASTLE POINT • HOBOKEN, NEW JERSEY 07030

85 09 09 032

Sputtering of Adsorbed Hydrogen

By Cesium Ion Bombardment

J. L. Lopes, J. A. Greer and M. Seidl

Department of Physics and Engineering Physics

PSPL8502

### Abstract

The production of negative hydrogen ions sputtered from a low work-function converter surface has been investigated. Hydrogen and cesium admitted into the vacuum chamber are chemisorbed on a polycrystalline molybdenum target.  $H^-$ ,  $Mo^-$ , and  $e^-$  are sputtered from this cathode by cesium ions in the energy range 250 to 1000 eV, and their angular distributions and parallel energy distributions are measured as a function of hydrogen gas pressure, cesium coverage and incident cesium ion energy. For optimum coverage, the  $H^-$  ion energy spread is about 0.5% of the incident cesium energy while the secondary electrons have an energy spread of about 0.04%. The spreads increase with decreasing coverage and are independent of surface roughness. The optimum  $H^-$ ,  $Mo^-$ , and  $e^-$  yields are also measured as a function of hydrogen pressure and incident cesium bombarding energy. The  $H^-$  ion optimum yield obtained was 0.4 for a cesium ion energy of 750 eV. The optimum  $Mo^-$  and  $e^-$  yields also incurred for a 750 eV cesium ion energy and are 0.15 and 0.18 respectively.

energy, a difference in parallel energy of approximately 0.27 eV was observed between high and low H<sub>2</sub> pressures. This spread is due to fringing dipole fields caused by patches in the cesium and hydrogen coverage.

Furthermore, the energy spreads are independent of surface roughness. This reflects the fact that the sputtered hydrogen atom undergoes a small number of atomic collisions close to the surface so that the sputtering process is unrelated to any large scale ordering of the surface topology.

An outgoing hydrogen atom can pick up an electron from the metal by resonant electron transfer and leave as H<sup>-</sup> ion. Hence, the sputtering yield of H<sup>-</sup> ions can be expressed as

$$\gamma(H^-) = \gamma(H^0)P \quad (15)$$

where  $\gamma(H^0)$  is the sputtering yield of hydrogen atoms and P is the ionization probability.

Measurements of the ionization have been obtained in FOM experiments [18,19,20] on scattering H<sup>+</sup> ions on cesiated tungsten surfaces. For cesiated W(110) a maximum value of P = 0.4 was found, and a maximum value of P = 0.25 was obtained for cesiated polycrystalline tungsten. Both maxima occur for a kinetic energy of approximately 10 eV in the direction perpendicular to the surface.

The largest sputtering yield  $\gamma(H^-) = 0.4$  occurred at a bombarding energy of 750 eV. In a previous experiment, Seidl and Pargellis [5] found that most H<sup>-</sup> ions leave the surface with a perpendicular energy equal to 1.3% of the Cs<sup>+</sup> energy. Thus, the optimum H<sup>-</sup> ion energy is 9.75 eV in agreement with FOM

#### IV. Discussion

The experimental data will be qualitatively discussed by means of a model described below.

In the optimum steady state, the Mo cathode is assumed to be covered with a monolayer of hydrogen which is in turn partially covered with cesium. A similar double layer on W(100) was examined by Papageorgopoulos and Chen [15]. They found that the coadsorption of hydrogen and cesium lowers the minimum workfunction from 1.6 eV to 1.4 eV and shifts the optimum coverage from 0.677 to 0.50 monolayers. We believe our minimum workfunction is 1.6 eV.

The sputtering of adsorbed hydrogen by energetic  $\text{Cs}^+$  ions occurs in binary collisions. A  $\text{Cs}^+$  ion knocks into an adsorbed hydrogen which is then reflected off the Mo lattice. Assuming elastic collisions the maximum energy transferrable to a hydrogen atom is

$$\frac{\Delta E}{E} = \frac{4 m_H M_{\text{Cs}}^+}{(m_H + M_{\text{Cs}})^2} \approx 3\% \quad (14)$$

Due to collisional statistics the  $\text{H}^-$  ion energy distribution is Maxwellian with a temperature of approximately 0.5 percent of the incident bombarding energy. These results are similar to the FWHM energy spread of 0.47% (0.7 eV spread at 150 eV) observed at the SITEX Negative Ion Source [16]. However, the Berkeley Source has a larger temperature of approximately 2.5% (5 eV spread at 200 eV). [17] The larger energy spread may be due to additional effects such as sputtering of  $\text{H}^-$  ions by  $\text{H}^+$  ions and backscattering of  $\text{H}^+$  ions.

The energy spreads are dependent upon hydrogen and cesium coverage. The temperature is larger when the coverage is incomplete. For each  $\text{Cs}^+$  bombarding

The optimum ion yield,  $H^-$ ,  $Mo^-$  and  $e^-$  yields as function of  $Cs^+$  bombarding energy is shown in Figure 21. The total ion yield rises linearly and reaches a maximum value of 0.56 at 750 eV. These values are similar to those obtained in an earlier experiment [6]. The  $H^-$  ion yield reaches a maximum value of 0.41 at 750 eV which agrees with the values obtained by Seidl and Pargellis [5].

where  $I_{Cs^+}$  is the bombarding current measured by the positive ion cup (Figure 3), the ion current  $I_{ION}$  is derived from integrating the angular distribution  $I(\theta)$  according to equation (1) and  $t = 0.733$  is the mesh transmission coefficient. For each set of data, the  $H^-$ ,  $Mo^-$ , and  $e^-$  integrated currents added to within a few percent of the rotating Faraday cup. This assured the correctness of all the measurements.

The maximum yield occurs when the target's workfunction is close to a minimum value [5,6,14]. In a previous work [6], the optimum total ion ( $H^-$  and  $Mo^-$ ) yields were obtained while monitoring the surface workfunction by a modified retarding field technique [11]. Differences in the workfunction were measured with respect to a thick cesium coated target surface. We assume that the workfunction for this well reproducible reference is close to 2.3 eV which was measured by Papageorgopoulos and Chen [15] for full coverage of co-absorbed hydrogen and cesium on tungsten (100). When the  $Cs^+$  ion bombardment is switched on the workfunction drops by about 0.6 eV for high enough hydrogen pressure, as shown in Figure 17. Once the minimum workfunction surface has been established it remains unchanged provided there is sufficient flux of cesium and hydrogen.

The optimum yields for  $H^-$ ,  $Mo^-$ , and  $e^-$  as function of  $H_2$  pressure and incident  $Cs^+$  energy are shown in Figures 18, 19, and 20 respectively. For each species, the yields reach a plateau above  $10^{-5}$  Torr and drop below this pressure. The yield's dependence on  $H_2$  pressure is caused by shifts in the workfunction. Figure 17 shows a 0.3 eV workfunction change between these gas pressures.

## B. Surface Roughness

The angular distribution as a function of surface roughness has been studied. A polycrystalline Mo insert was polished using  $0.5\mu \text{ Al}_2\text{O}_3$  powder to a mirror finish as shown in Figure 10. The insert was then exposed to the sputtering process. Figure 11 illustrates the sputtered surface after a  $\text{Cs}^+$  dosage of  $3.6 \times 10^{18}$  ions/cm<sup>2</sup>, and Figure 12 shows the roughened target after a  $\text{Cs}^+$  dosage of approximately  $10^{19}$  ions/cm<sup>2</sup>.

Periodically, angular distributions were taken of sputtered  $\text{H}^-$  ions and secondary  $e^-$  while the insert was undergoing the sputtering process. Figures 13 and 14 show these particles angular distributions to be independent of surface roughness. This agrees with studies done at Los Alamos National Laboratory [13]. Hence, polished target surfaces are not needed for every angular distribution measurement. The energy spreads are shown in Figures 15 and 16 where a least-squares fit to the straight lines give a  $\text{H}^-$  ion temperature of approximately .5% and an  $e^-$  temperature of approximately 0.04% of the incident bombarding energy for the various target surfaces.

## C. Yield Measurements

The negative ion yield is defined as the number of negative ions sputtered per incident cesium ion:

$$\gamma = \frac{J_{\text{ION}}}{J_{\text{Cs}^+}} \quad (12)$$

where  $J_{\text{ION}}$  is the current density of the sputtered ions and  $J_{\text{Cs}^+}$  is the cesium ion current density. Thus the negative ion yield can be obtained from

$$\gamma = \frac{I_{\text{ION}}}{t I_{\text{Cs}^+}} \quad (13)$$

incomplete hydrogen coverage the temperature increases. This increase is approximately 0.27 eV for all bombarding energies. The fact that the temperature increase is independent of bombarding energy indicates that the additional spread is due to fringing dipole fields caused by patches of hydrogen and cesium coverage. Similar results are seen when the cesium coverage is reduced. Table 1 illustrates the effects of cesium and hydrogen coverage upon the temperature.

The temperature increase due to patch formations is especially important at low bombarding energies for which the H<sup>-</sup> ion spread due to sputtering is small.

The e<sup>-</sup> angular distribution is approximately Gaussian,

$$f(\theta) \sim e^{-(\theta/\theta_0)^2} \quad (10)$$

where  $\theta_0 \sim 1.2^\circ$  independent of Cs<sup>+</sup> energy. Using equation (6), the e<sup>-</sup> parallel energy distribution can be shown to be Maxwellian

$$f(E_{||}) \sim e^{-E_{||}/T} \quad (11)$$

with an ion temperature T of approximately .04% of the incident Cs<sup>+</sup> bombarding energy. These e<sup>-</sup> temperatures are similar to those observed at Los Alamos National Laboratory [13].

Table 2 is a summary of the H<sup>-</sup> ion and e<sup>-</sup> optimum coverage temperatures for various Cs<sup>+</sup> bombarding energies.

Since  $U \gg E_{\parallel}$

$$\tan^2 \theta \sim E_{\parallel} / U \quad (7)$$

Therefore, the sputtered particle's parallel energy may be obtained by measuring the angle  $\theta$ .

The angular distribution of an ion species is a plot of the current  $I(\theta)$  measured by the magnetic spectrometer as function of the angle  $\theta$ . A typical set of  $H^-$ ,  $Mo^-$ , and  $e^-$  angular distributions for various  $Cs^+$  bombarding energies are shown in Figures 5, 6, and 7 respectively.

Measurements indicate that the  $H^-$  ion angular distribution is Gaussian,

$$f(\theta) \sim e^{-\left(\theta/\theta_0\right)^2} \quad (8)$$

where  $\theta_0$  varies between  $3.2^\circ$  to  $4.5^\circ$  approximately independently of  $Cs^+$  bombarding energy. Using equation (7), the angular distribution can be converted into the parallel energy distribution. Figure 8 illustrates that the  $H^-$  ion parallel energy distribution is Maxwellian,

$$f(E_{\parallel}) \sim e^{-E_{\parallel}/T} \quad (9)$$

with an ion temperature  $T$ . The temperature is found by utilizing a least squares fit for the slope of the lines in Figure 8.

The results show that the  $H^-$  ion temperature is a minimum when the hydrogen and cesium coverage is the largest. Figure 9 illustrates the dependence of the  $H^-$  temperature upon  $H_2$  pressure for a variety of  $Cs^+$  bombarding energies. For a particular energy these temperatures appear to be constant for  $H_2$  pressures higher than  $10^{-5}$  Torr. For lower  $H_2$  pressure corresponding to an

### III. Experimental Results

#### A. Angular Distribution

Due to collisions during the sputtering process, the negative ions will leave the target with initial velocities which will have components parallel and perpendicular to the target surface. The parallel velocity component will make the negative ion trajectories parabolic in the region between the target and mesh as seen in Figure 4.

A sputtered particle will have initial parallel and perpendicular energy given by

$$E_{\perp} = \frac{1}{2} m v_{\perp}^2 \quad (2)$$

and

$$E_{\parallel} = \frac{1}{2} m v_{\parallel}^2 \quad (3)$$

respectively,  $v_{\perp}$  is the initial perpendicular velocity,  $v_{\parallel}$  is the initial parallel velocity. As the sputtered particle exits the cesium manifold's aperture, it will have a final parallel and perpendicular velocity component  $v'_{\parallel}$  and  $v'_{\perp}$  respectively which define an angle  $\theta$ . The final energies are given by

$$\frac{1}{2} m v'_{\perp}^2 = E_{\perp} + U \quad (4)$$

and

$$\frac{1}{2} m v'_{\parallel}^2 = E_{\parallel} \quad (5)$$

where  $U$  is the accelerating voltage applied between the mesh and target.

Thus,

$$\tan^2 \theta = \left( \frac{v'_{\parallel}}{v'_{\perp}} \right)^2 = \frac{E_{\parallel}}{E_{\perp} + U} \quad (6)$$

Fine alignment was accomplished via a spring adjustment assembly. The alignment was confirmed first by a pair of deflector plates positioned at the rear of the diode, and second by comparing the sum of the integrated currents for each species with the current collected by the total yield Faraday cup.

Assuming rotational symmetry for the beamlet, the integrated current for a particular ion species is given by

$$I = 2 \left(\frac{R}{R_0}\right)^2 \int_0^{\pi/2} I(\theta) \sin\theta d\theta = 1.07 \times 10^5 \int_0^{\pi/2} I(\theta) \sin\theta d\theta \quad (1)$$

Here  $I(\theta)$  is the current measured by the Faraday cup of the magnet.  $\theta$  is the angular position of the acceptance aperture of the magnet with respect to the normal to the cathode.  $R_0 = .317$  mm is the radius of the magnet's acceptance aperture.  $R = 7.33$  cm is the distance between the cesium manifold's aperture and the magnet's entrance aperture.

The stripping cross sections for  $H^-$  range from  $\sim 6 \times 10^{-16}$   $cm^2$  to  $\sim 10 \times 10^{-16}$   $cm^2$  for ion energies of 200 to 1000 eV [12]. Thus, at high  $H_2$  pressure ( $\sim 10^{-4}$  Torr) there is some ion current attenuation. This effect is no more than 10% and has been taken into account when obtaining the  $H^-$  integrated current.

Hydrogen and cesium are coadsorbed on a molybdenum target surface, and  $H^-$ ,  $Mo^-$ , and  $e^-$  are sputtered by  $Cs^+$  ion bombardment. These negatively charged particles are accelerated back across the diode gap, partially attenuated by the mesh and collected by the cesium manifold. A small sample of the sputtered beam passes through two apertures defining a cone of  $14^\circ$  half angle and is then presented to the diagnostic apparatus.

The diagnostic apparatus consists of a Faraday cup and a mass spectrometer. The Faraday cup measures the total current due to all ( $H^-$ ,  $Mo^-$ , and  $e^-$ ) negative particles. A negatively biased guard ring prevents any secondary electrons from leaving the cup. This Faraday cup can then be rotated out of the beamlet's path so that the beamlet can be analyzed using the mass spectrometer.

A  $28^\circ$  magnetic sector mass spectrometer with a resolution of  $\sim 20$  and a gap width of  $\sim 6$  mm was constructed to obtain angular distributions of  $H^-$ ,  $Mo^-$  ions, and electrons. The magnet was mounted onto a frame which rotated about the cesium manifold's aperture. The mass spectrometer's entrance aperture (.635 mm diameter) and the cesium manifold's aperture (.635 mm diameter) define a  $\sim 43$  milliradian acceptance angle of the ion beam into the magnetic field region. An exit slit of 5 mm width allowed for the detection of the individual ion species. A Faraday cup placed behind the exit slit collected all of the ions of a particular species admitted into the magnetic field region. Secondary electrons were suppressed from leaving the cup by placing a negatively biased guard ring between the exit slit and the Faraday cup.

The magnet's acceptance aperture was mechanically aligned at the same height above the vacuum chamber's base as the cesium manifold's aperture.

is broken by bending the stainless steel bellows which is welded into the chamber.

The cesium manifold is heated to 300°C and has two exit channels of 0.010" wide by 2.375" long by which cesium vapor can diffuse through. The manifold provides a uniform flux of cesium vapor to the diode region. Some of the cesium is surface ionized at the hot tungsten mesh which acts as a source of Cs<sup>+</sup> ions. These ions are accelerated onto the negatively biased cathode. The Cs<sup>+</sup> ion current density is measured by two positive ion cups facing two .635 mm diameter holes drilled in the molybdenum alignment plate. The specific permeance of the cathode is large enough to provide a space-charge limited Cs<sup>+</sup> ion current density of 100  $\mu\text{A}/\text{cm}^2$  at 100 V. This corresponds to a flux of Cs<sup>+</sup> ions almost two orders of magnitude larger than the residual water vapor flux. The lens effect of the mesh adds an intrinsic angular spread of 7.5 milliradians to the negative ions accelerated by the mesh [7,8].

Cesium coverage of the cathode is varied by changing the ratio of the cesium ion to atom fluxes which is accomplished by varying the mesh temperature. In an initial experiment [6], a modified retarding electric field technique was used to obtain the relative workfunction of the cathode [9,10,11] while undergoing the sputtering process. This method utilized a collimated electron beam produced by a Model 4760 A-HR high resolution electron gun (Apex Corporation). This procedure consisted of obtaining characteristic I-V plots of an electron current collected by the cathode from which the relative workfunction would be obtained. A schematic of this arrangement is shown in Figure 3.

## **II. Experimental Apparatus**

The experimental apparatus consists of a vacuum system, a planar diode, a Faraday cup assembly, and a rotating mass spectrometer as shown in Figure 1.

The vacuum system is evacuated by a six inch oil diffusion pump and a methanol cooled baffle (-30°C) to a background pressure in the  $10^{-8}$  Torr range measured with a Veeco RG-840 ionization gauge. While in operation, the chamber is backfilled with hydrogen gas (99.999% purity) from  $1 \times 10^{-6}$  Torr to  $2.4 \times 10^{-4}$  Torr. The gas is admitted into the vacuum system from a gas cylinder via a Granville-Phillips series 203 variable leak valve.

The main part of the experiment is a planar diode shown in Figure 2. The cathode of the diode consists of a polycrystalline molybdenum insert placed at the center of a molybdenum alignment plate. With this cathode, data from various target surfaces can easily be obtained. The cathode is mounted onto an oxygen free copper cooling block, and typical cathode operating temperature ranges from 35 to 45°C.

The anode is comprised of a fine tungsten mesh (180 wires per inch with 0.0008" wire diameter) placed 2.0 mm from the cathode. The tungsten mesh is mounted onto the rear anode and is aligned with the front anode. During operation the mesh is heated to about 1000°C by passing 3 to 4 amps of current through it.

Cesium vapor is produced in a small oven heated to 150°C and directed into a cesium manifold by means of a feeder tube heated to 300°C. The cesium oven is a stainless steel chamber into which is placed a glass ampoule containing 2 grams of cesium. After the oven has been evacuated, the ampoule

from 500 to 1250 eV. In experiment [6] the sputtering yield was measured for the energy range 150 to 900 eV but no energy distribution of the H<sup>-</sup> ions has been measured.

In this work we present measurements of angular (and energy) distribution of sputtered H<sup>-</sup> and Mo<sup>-</sup> ions and of electrons in the bombarding energy range of 250 to 1000 eV. By integrating the angular distributions, more precise data on sputtering yields are obtained. Effects of surface roughness and of incomplete cesium or hydrogen coverage on angular spread of the sputtered ions are also studied.

## I. Introduction

In a negative hydrogen ion the electron is bound to the hydrogen atom with an energy of 0.75 eV [1]. The small binding energy makes it relatively easy to detach the outer electron from the atom after accelerating the negative ion to high energies [2]. Negative hydrogen ions are thus the necessary ingredient for producing beams of energetic hydrogen atoms.

It has been shown by many authors that negative hydrogen ions can be produced on the surface of a metallic target placed into a hydrogen-cesium plasma and negatively biased with respect to the plasma [3]. Surface production of negative hydrogen ions may be due to the following processes:  
a) backscattering hydrogen ions or atoms from the target surface, b) sputtering adsorbed or implanted hydrogen from the target by cesium or hydrogen bombardment [4]. In order to study a particular process it is necessary to set up experimental conditions in which only that process can occur.

In two previous experiments [5,6] we have studied sputtering of adsorbed hydrogen from a cesiated molybdenum target bombarded with cesium ions. The target is exposed to a flux of cesium atoms and cesium ions. By changing the ratio of these two fluxes the cesium coverage of the target (determining the workfunction) can be controlled. The target is also exposed to hydrogen gas. Hydrogen atoms are chemisorbed on the target. Hydrogen coverage is controlled by gas pressure.

In experiment [5] we have measured the sputtering yield (yield is defined by the number of  $H^-$  ions produced per incident  $Cs^+$  ion) of negative hydrogen ions and their energy distribution for  $Cs^+$  ion bombardment energy ranging

experiments [18,19,20]. For  $P = 0.25$  and using equation (15) a total sputtered yield of  $\gamma(H^0) = 1.6$  must be assumed.

The small yields of  $H^-$  ions for  $Cs^+$  ion energies below 250 eV indicate that sputtering of adsorbed hydrogen by  $Cs^+$  ion bombardment can account for only a fraction of the  $H^-$  ions produced in surface conversion sources that usually operate at 100 to 200 eV. The hydrogen plasma in contact with the converter surface may cause three additional effects. Sputtering of  $H^-$  ions will be caused by  $H^+$  ion bombardment, and backscattering of  $H^+$  ions will also produce  $H^-$  ions. However, these two mechanisms for  $H^-$  production result in a high  $H^-$  ion temperature. Hydrogen ion implantation may substantially increase the hydrogen concentration close to the converter surface [21] which may increase the total sputtering yield( $\gamma H^0$ ). Currently, an experiment is being built to study effects of ion implantation on  $H^-$  ion production.

Acknowledgements

We wish to thank Raymond Gibson for designing the rotating mass spectrometer, and G. Wohlrab and G. Wirth for building most of the experimental apparatus.

This work is supported by AFOSR Grant 83-0230 and DOE Grant DE-AC02-84ER-53167.

## References

1. H. & W. Massey, Negative Ions. Cambridge University Press (1976).
2. Neutralization. Production and Neutralization of Negative Ions and Beams (K. Prelec, Editor), American Institute of Physics Proceedings, Number 111 (1984) pp. 547-584.
3. Negative Ion Sources. Production and Neutralization of Negative Ions and Beams (K. Prelec, Editor), American Institute of Physics Proceedings, Number 111 (1984) pp. 331-470.
4. Surface Production. Production and Neutralization of Negative Ions and Beams (K. Prelec, Editor), American Institute of Physics Proceedings, Number 111 (1984) pp. 171-288.
5. M. Seidl and A. Pargellis, Phys. Rev. B26, 1 (1982).
6. J. A. Greer, M. Seidl, Sputtering Yields of Negative Hydrogen Ions. Production and Neutralization of Negative Ions and Beams (K. Prelec, Editor), American Institute of Physics Proceedings, Number 111 (1984) p.220.
7. J. Ard Simpson, Reviews of Scientific Instruments 32, 1283 (1961).
8. G. Slodyian, NBS, Spec. Pub. 427, Workshop on Secondary Ion Mass Spectrometry and Ion Microprobe Mass Analysis held at NBS, Gaithersburg, Maryland, Sept. 16-18, 1974.
9. H. Shelton, Phys. Rev. 107, 1553 (1957).
10. G. A. Haas, R. E. Thomas, Surface Science 4, 64 (1968).
11. A. G. Knapp, Surface Science 34, 289 (1973).
12. J. S. Risley, R. Geballe, Phys. Rev. A9, #6 (1974).
13. Private communications with Dr. Ralph Stevens.
14. M. Yu, Phys. Rev. Letters 40, 574 (1978).
15. C. A. Papageorgopoulos, J. M. Chen, Surface Sci., 39, 283 (1973).
16. W. L. Sterling, W. K. Dagenhart, J. J. Donaghy, Normalized Emittance of SITEX Negative Ion Source. Production and Neutralization of Negative Ions and Beams (K. Prelec, Editor), American Institute of Physics Proceedings, Number 111 (1984) p. 220.

17. A. F. Lietzke, B. O. Yant, K. W. Ehlers, The Parametric Dependence of H<sup>-</sup> (D<sup>-</sup>) Spatial Profiles from a Surface Conversion Source. Bull. Amer. Phys. Soc. 29, 1312 (Oct. 1984).
18. J. N. M. van Wunnic, J. J. C. Geerlings and J. Los, Surface Sci. 131, 1 (1983).
19. J. N. M. van Wunnic, J. J. C. Geerlings, E. H. A. Granneman and J. Los, Surface Sci. 131, 17 (1983).
20. P. J. M. van Bommel, J. J. C. Geerlings, J. N. M. van Wunnic, P. Messmann, E. H. A. Granneman, and J. Los, J. Appl. Phys. 54, 5676 (1983).
21. M. Seidl, A. N. Pargellis, J. Greer, Proc. of the U.S.-Mexico Joint Seminar on the Atomic Physics of Negative Ions, Edited by C. Cisneros and T. J. Morgan (Instituto de fisica, UNAM, Mexico, 1982) p. 393.

### Figure Captions

- Figure 1. Schematic diagram of experimental apparatus in vacuum chamber.
- Figure 2. Diagram of experimental planar diode.
- Figure 3. Cross section of experimental apparatus used for total ion yield and workfunction measurements.
- Figure 4. The effect of intrinsic energy spread on ion trajectories.
- Figure 5.  $H^-$  ion angular distribution for various  $Cs^+$  ion energies for optimum cathode workfunction. Hydrogen pressure is  $2.4 \times 10^{-4}$  Torr in all cases.
- Figure 6.  $Mo^-$  ion angular distributions for various  $Cs^+$  ion energies for optimum cathode workfunction. Hydrogen pressure is  $2.4 \times 10^{-4}$  Torr in all cases.
- Figure 7.  $e^-$  ion angular distributions for various  $Cs^+$  ion energies for optimum cathode workfunction. Hydrogen pressure is  $2.4 \times 10^{-4}$  Torr in all cases.
- Figure 8.  $H^-$  ion parallel energy distribution for various  $Cs^+$  ion energies for optimum workfunction. The abscissa is the  $H^-$  ion energy divided by the  $Cs^+$  ion energy. Hydrogen pressure is  $2.4 \times 10^{-4}$  Torr in all cases.
- Figure 9. The  $H^-$  ion temperature as function of hydrogen pressure and  $Cs^+$  ion energy for optimum cathode workfunction.
- Figure 10. SEM picture of a polished Mo sputtering surface magnified 500 times.
- Figure 11. SEM picture of a sputtered Mo surface magnified 500 times. The target was sputtered with a  $Cs^+$  dosage of  $3.6 \times 10^{18}$  ions/cm<sup>2</sup>.
- Figure 12. SEM picture of a sputtered Mo surface magnified 500 times. The target was sputtered with a  $Cs^+$  dosage of approximately  $10^{19}$  ions/cm<sup>2</sup>.

Figure 13.  $H^-$  angular distribution as a function of surface roughness for a  $Cs^+$  energy of 300 eV. Hydrogen pressure is  $1.44 \times 10^{-4}$  Torr in all cases.

Figure 14.  $e^-$  angular distribution as a function of surface roughness for a  $Cs^+$  energy of 300 eV. Hydrogen pressure is  $1.44 \times 10^{-4}$  Torr in all cases.

Figure 15.  $H^-$  ion parallel energy distribution as a function of surface roughness for a  $Cs^+$  energy of 300 eV. Hydrogen pressure is  $1.44 \times 10^{-4}$  Torr in all cases.

Figure 16.  $e^-$  ion parallel energy distribution as a function of surface roughness for a  $Cs^+$  energy of 300 eV. Hydrogen pressure is  $1.44 \times 10^{-4}$  Torr in all cases.

Figure 17. The effect of  $H_2$  pressure and  $J_{Cs^+}$  on the surface workfunction.

Figure 18.  $H^-$  ion yield as function of hydrogen pressure and  $Cs^+$  ion energy for optimum cathode workfunction.

Figure 19.  $Mo^-$  ion yield as function of hydrogen pressure and  $Cs^+$  ion energy for optimum cathode workfunction.

Figure 20.  $e^-$  yield as function of hydrogen pressure and  $Cs^+$  ion energy for optimum cathode workfunction.

Figure 21. Optimum total ion,  $H^-$ ,  $Mo^-$ , and  $e^-$  yield as function of  $Cs^+$  ion energy.

$H_2$ Pressure (Torr)	Over Cesiumated (T/U) x 100%	Optimum Coverage (T/U) x 100%	Under Cesiumated (T/U) x 100%
$4.8 \times 10^{-4}$	.38	.44	.48
$2.4 \times 10^{-4}$	.39	.44	.48
$4.8 \times 10^{-5}$	.42	.44	.51
$1.68 \times 10^{-5}$	.42	.44	.55

Table 1. The effects of hydrogen and cesium coverage on the  $H^-$  ion temperature. The  $Cs^+$  energy is 500 eV in all cases.

U(eV)	$H^-$		electrons	
	$\theta_0$ (Deg)	(T/U) x 100%	$\theta_0$ (Deg)	(T/U) x 100%
250	4.44	0.60	1.17	0.042
300	4.15	0.53	1.17	0.042
350	4.05	0.50	1.19	0.043
400	3.86	0.46	1.23	0.046
450	3.83	0.45	1.19	0.043
500	3.77	0.43	1.17	0.042
625	3.58	0.39	1.16	0.041
750	3.46	0.37	1.15	0.040
900	3.35	0.34	1.15	0.040
1000	3.24	0.32	1.13	0.039

Table 2. The  $H^-$  ion and  $e^-$  angular spreads and their corresponding temperatures for various  $Cs^+$  energies. Hydrogen pressure is  $2.4 \times 10^{-4}$  Torr.

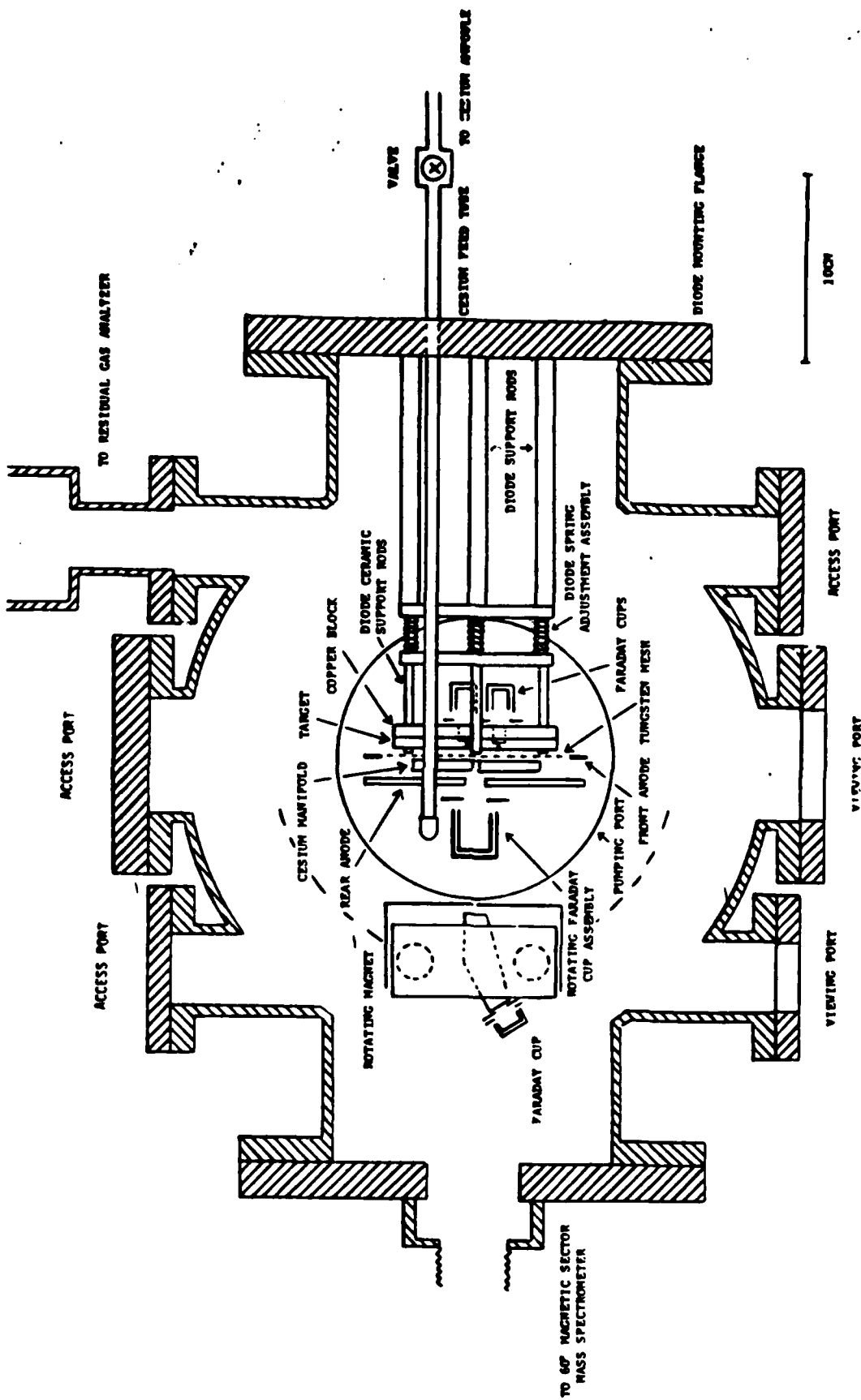


Figure 1. Schematic diagram of experimental apparatus in vacuum chamber.

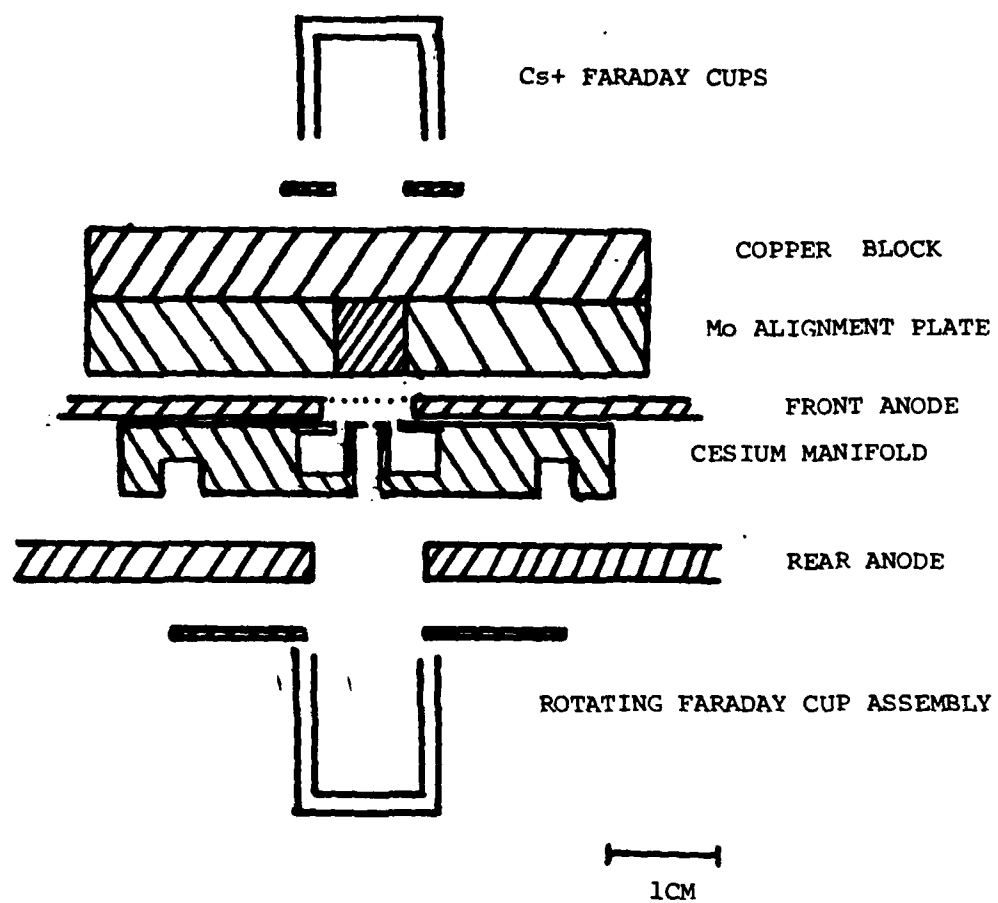
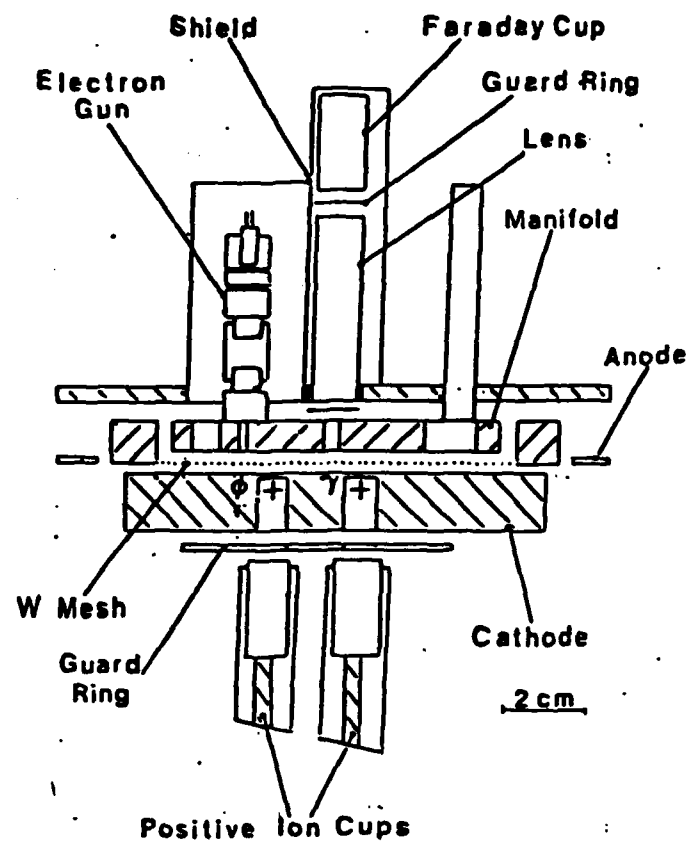


Figure 2. Diagram of experimental planar diode.



**Figure 3. Cross section of experimental apparatus used for total ion yield and workfunction measurements.**

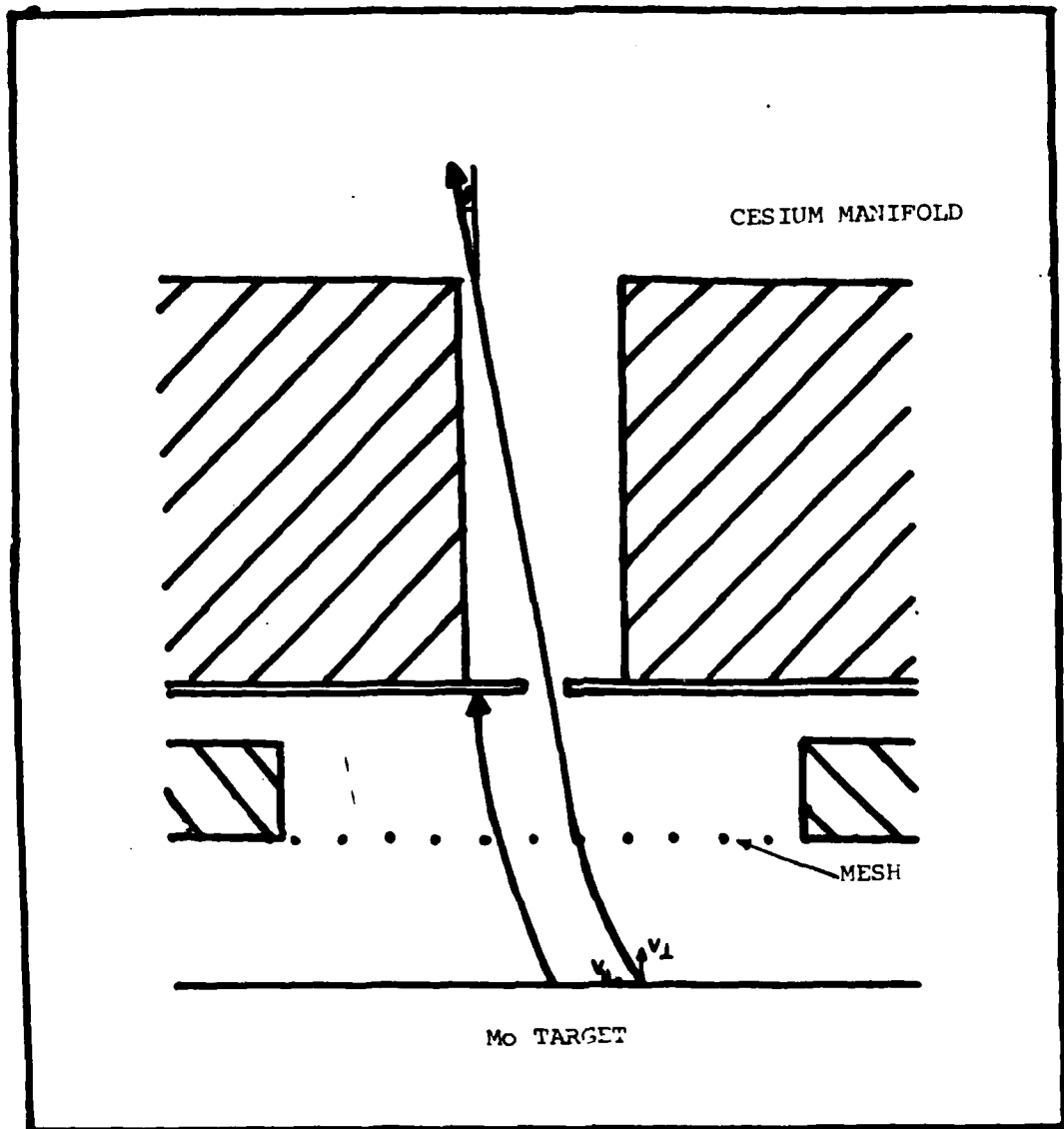


Figure 4. The effect of intrinsic energy spread on ion trajectories.

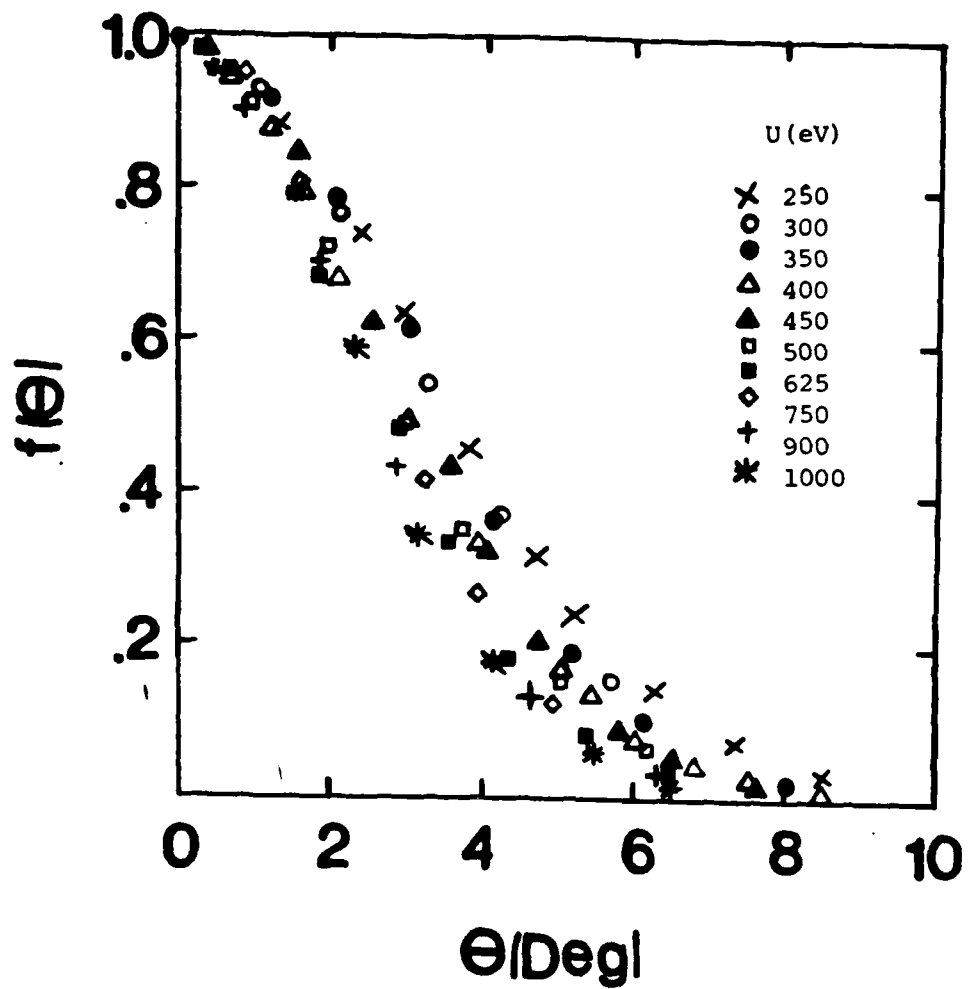


Figure 5.  $H^+$  ion angular distribution for various  $Cs^+$  ion energies for optimum cathode workfunction. Hydrogen pressure is  $2.4 \times 10^{-4}$  Torr in all cases.

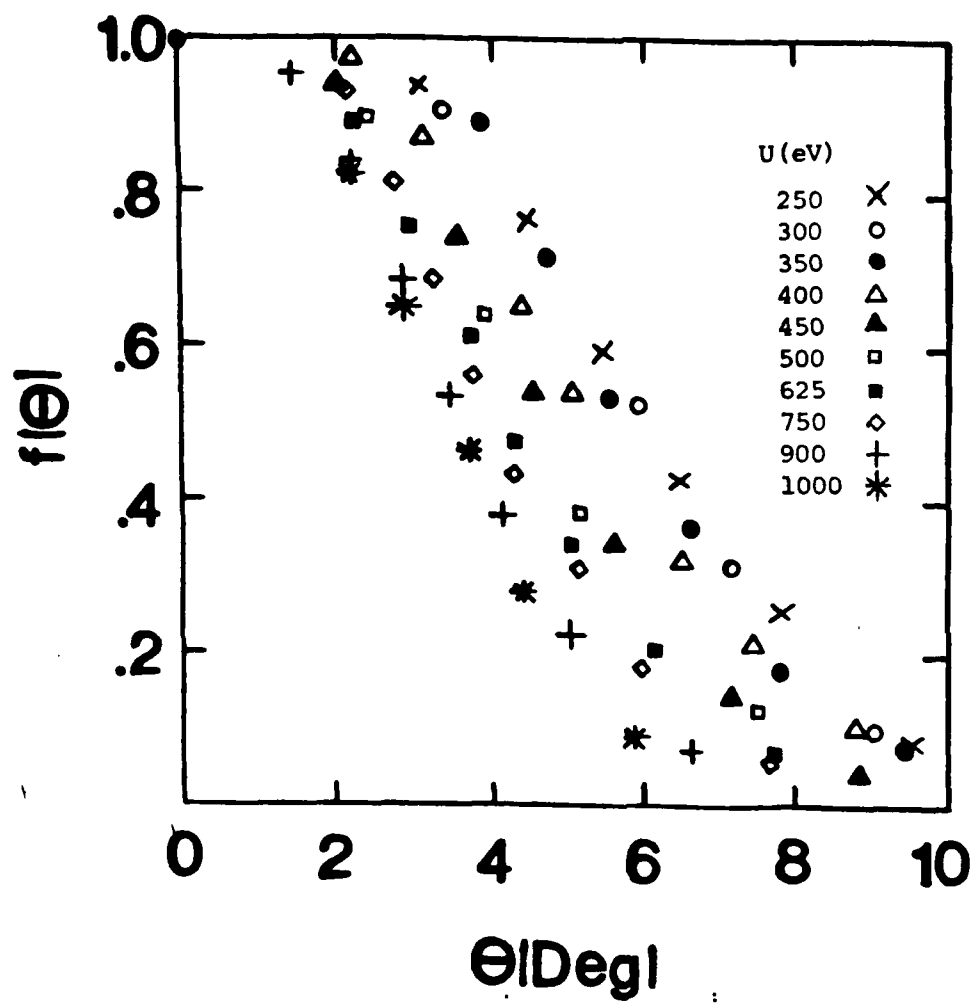


Figure 6.  $\text{Mo}^+$  ion angular distributions for various  $\text{Cs}^+$  ion energies for optimum cathode workfunction. Hydrogen pressure is  $2.4 \times 10^{-4}$  Torr in all cases.

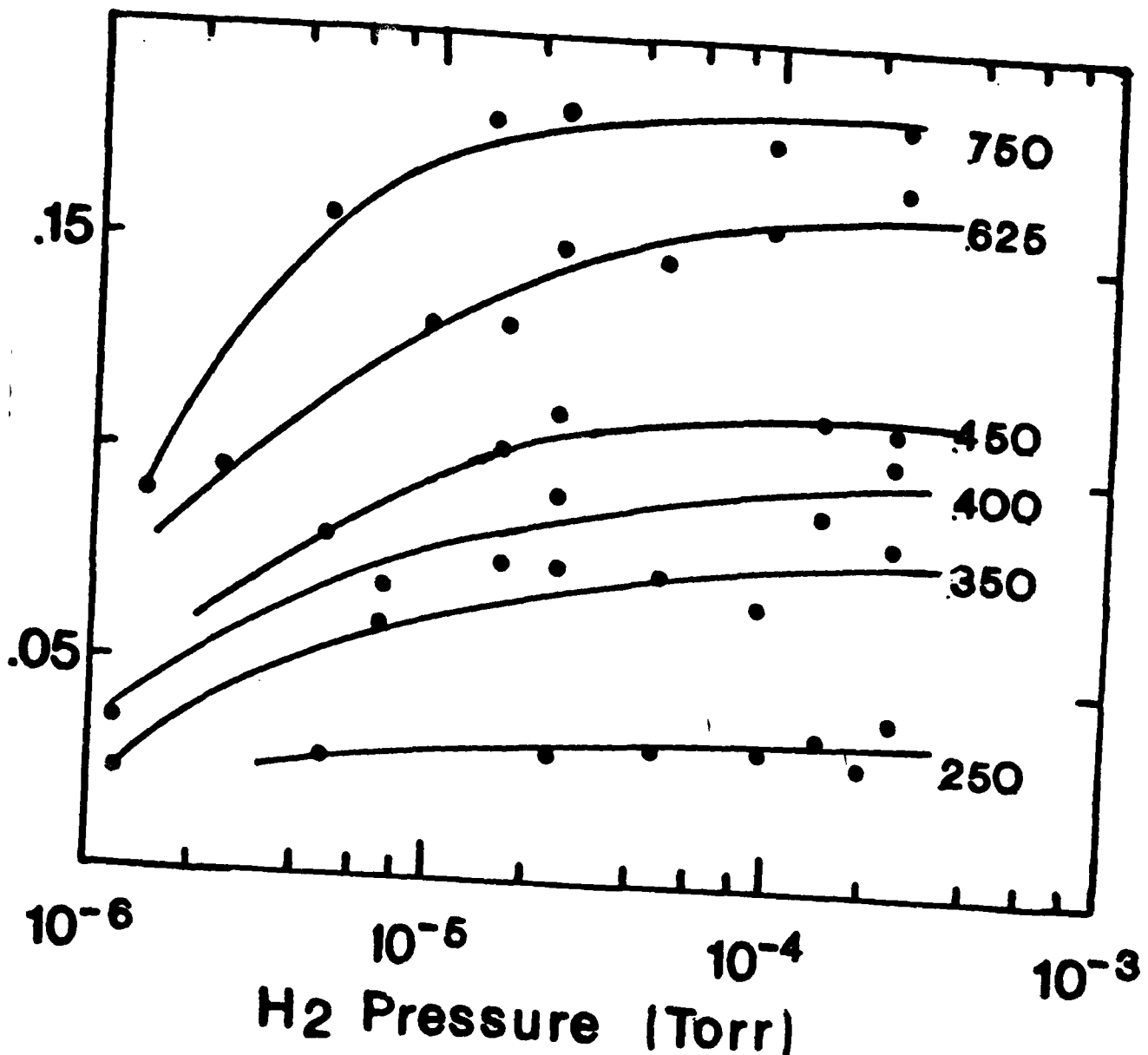


Figure 20. e<sup>-</sup> yield as function of hydrogen pressure and Cs<sup>+</sup> ion energy for optimum cathode workfunction.

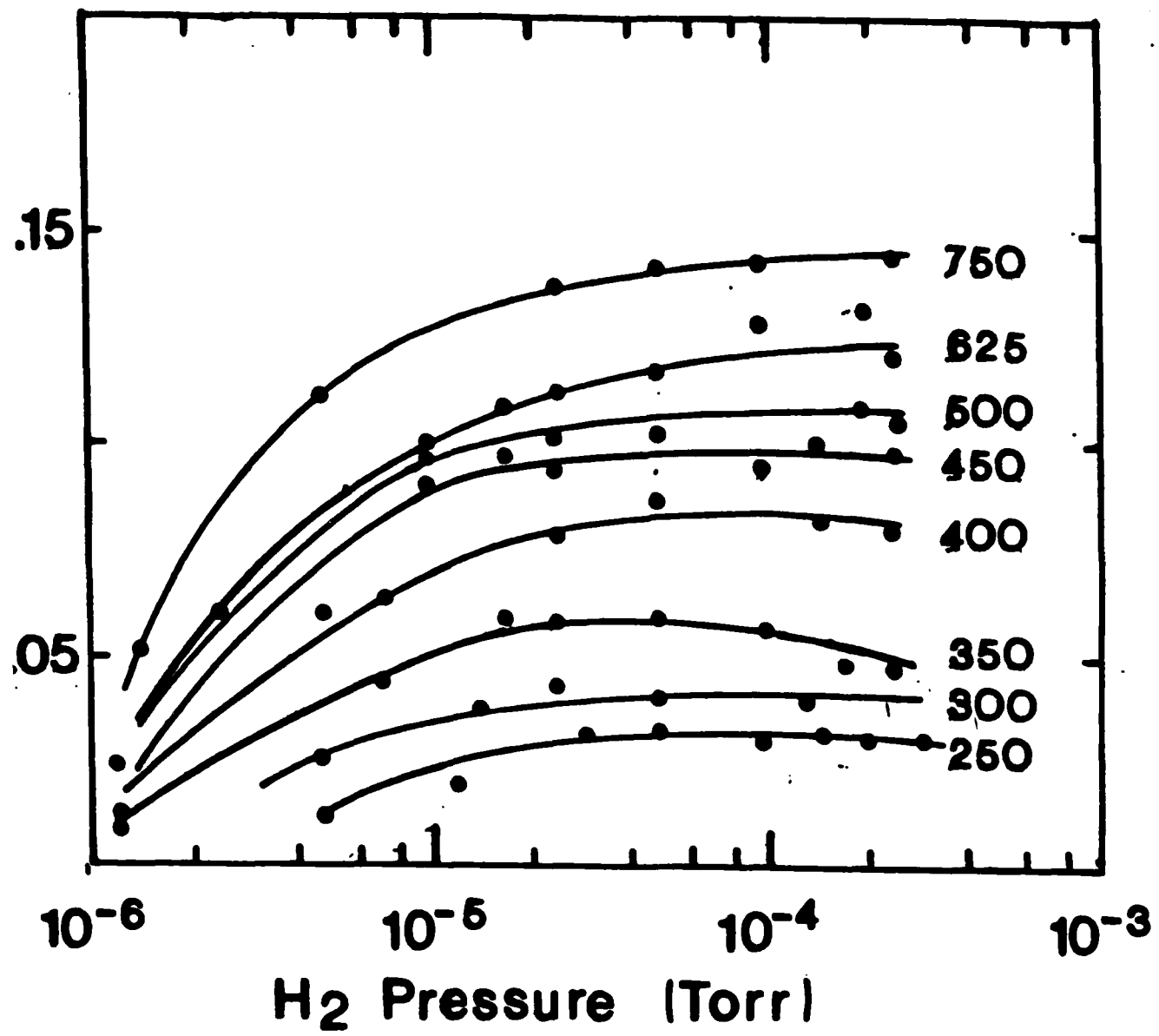


Figure 19.  $\text{Mo}^+$  ion yield as function of hydrogen pressure and  $\text{Cs}^+$  ion energy for optimum cathode workfunction.

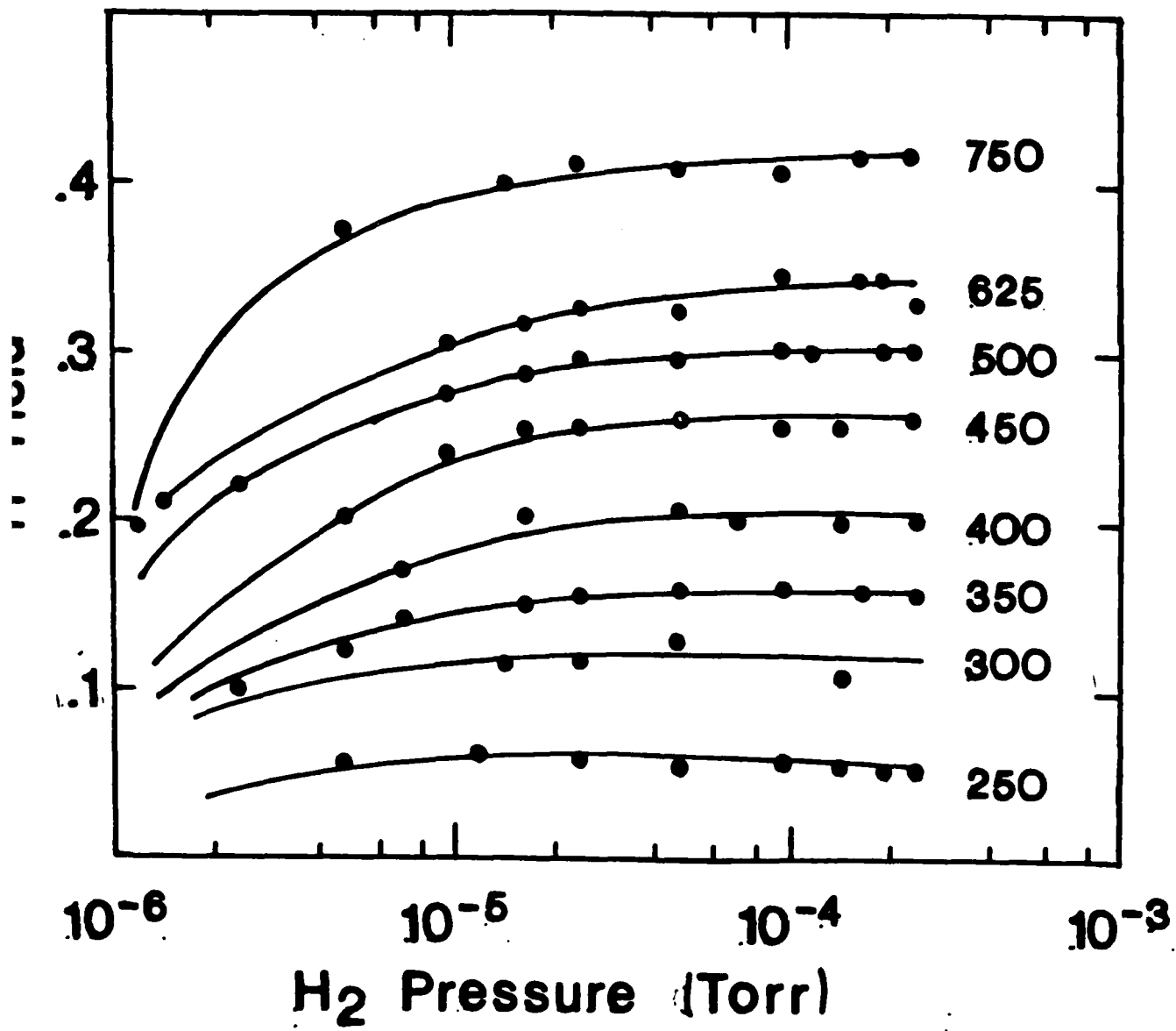


Figure 18. H<sup>-</sup> ion yield as function of hydrogen pressure and Cs<sup>+</sup> ion energy  
for optimum cathode workfunction.

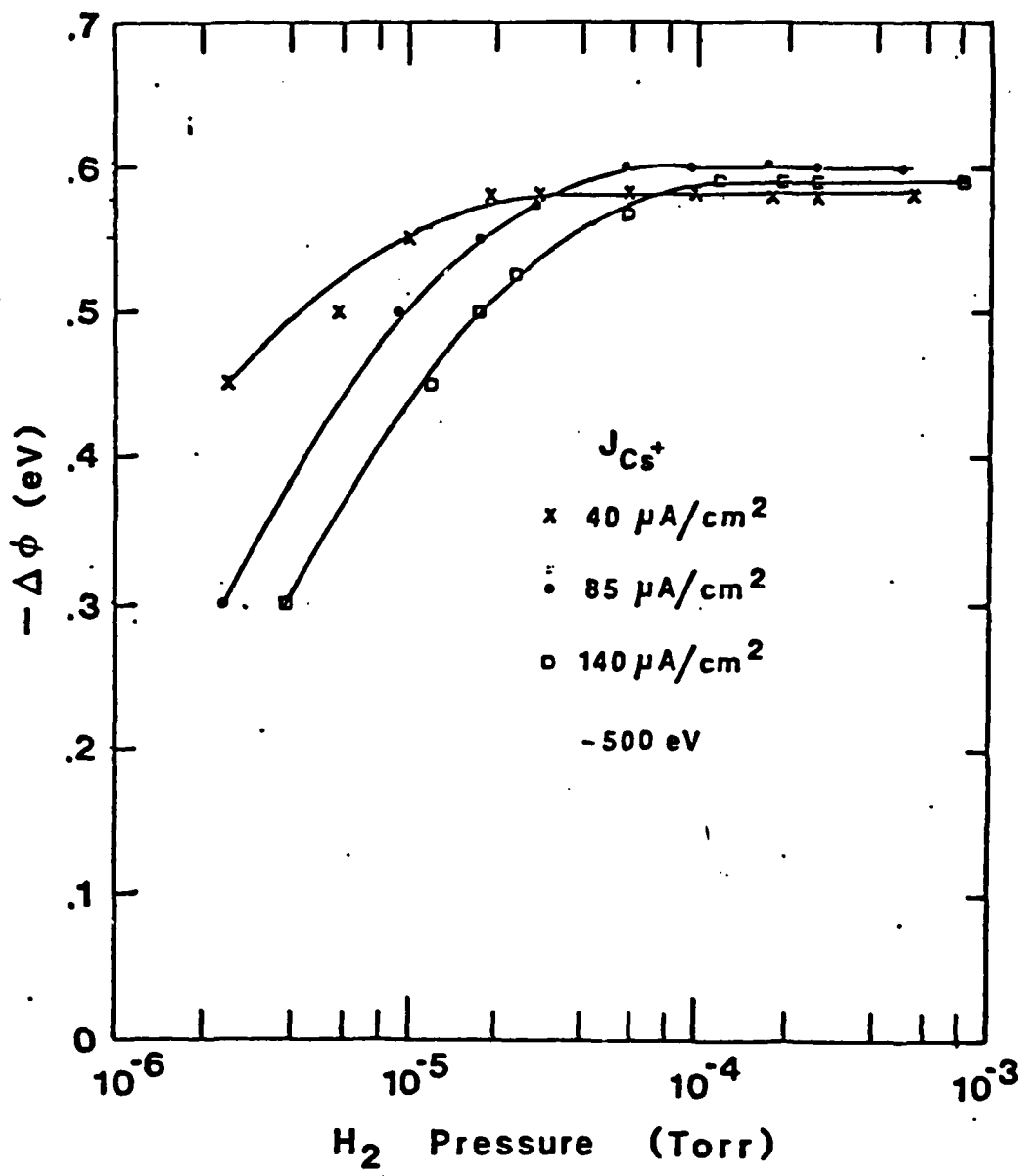
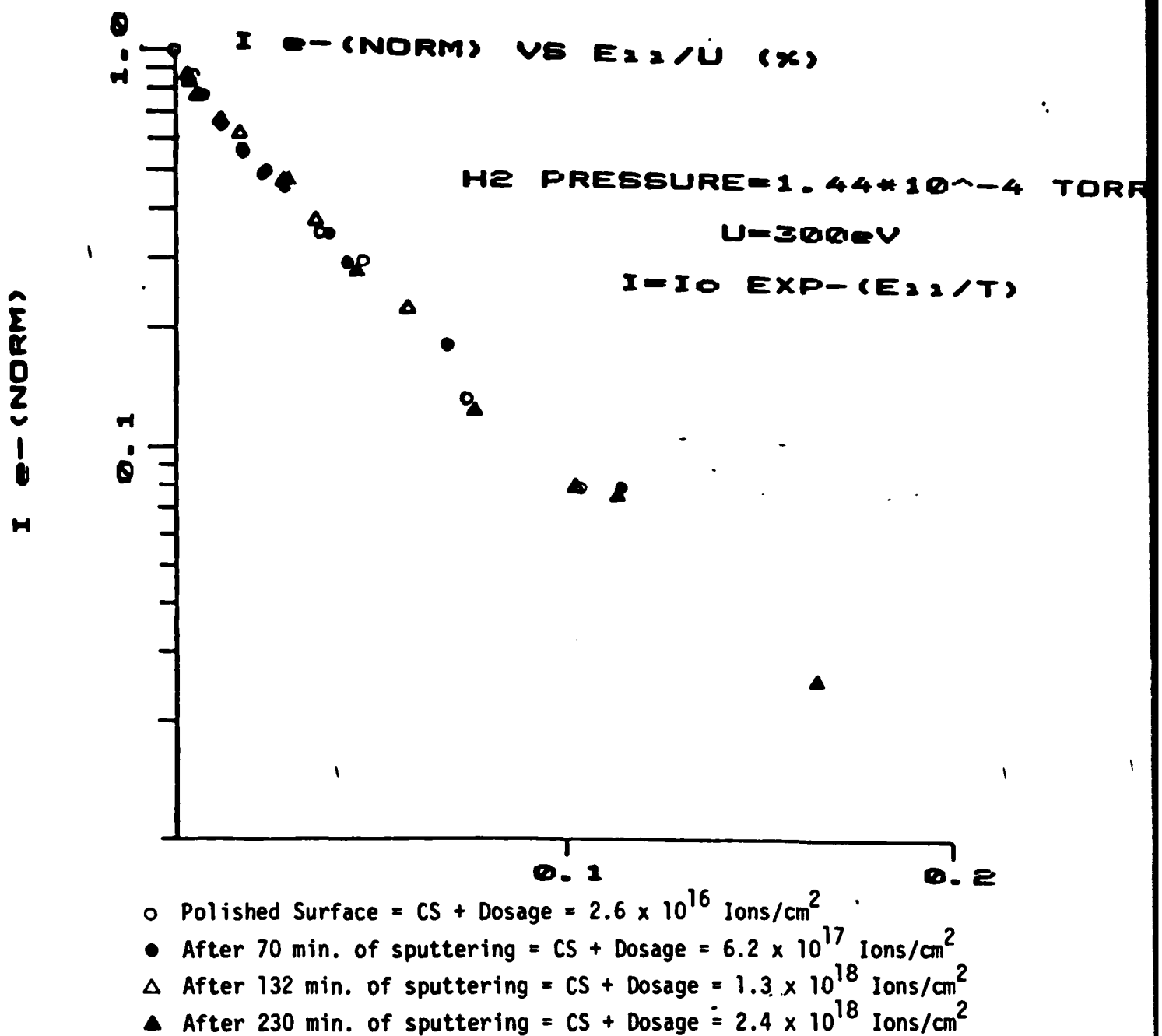


Figure 17.: The effect of true  $H_2$  pressure and  $J_{Cs^+}$  on the surface work function.



**Figure 16.**  $e^-$  ion parallel energy distribution as a function of surface roughness  
 for a Cs<sup>+</sup> energy of 300 eV. Hydrogen pressure is  $1.44 \times 10^{-4}$  Torr  
 in all cases.

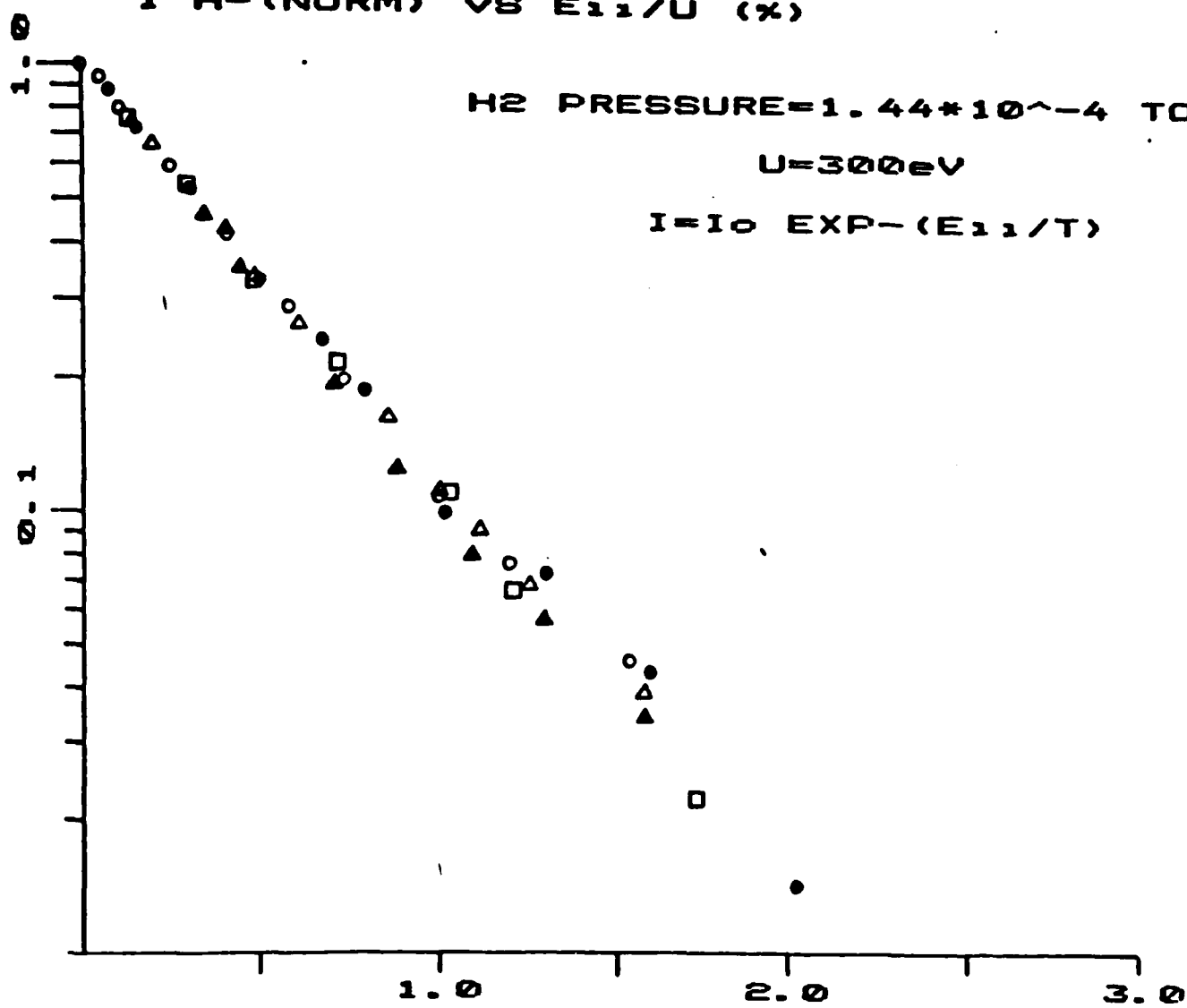
I H-(NORM) VS E<sub>z,z</sub>/U (%)

H<sub>2</sub> PRESSURE =  $1.44 \times 10^{-4}$  TORR

U = 300 eV

I = I<sub>0</sub> EXP - (E<sub>z,z</sub>/T)

I H-(NORM)



E<sub>z,z</sub>/U (%)

- Polished Surface = CS + Dosage =  $2.6 \times 10^{16}$  Ions/cm<sup>2</sup>
- After 70 min. of sputtering = CS + Dosage =  $6.2 \times 10^{17}$  Ions/cm<sup>2</sup>
- △ After 132 min. of sputtering = CS + Dosage =  $1.3 \times 10^{18}$  Ions/cm<sup>2</sup>
- ▲ After 230 min. of sputtering = CS + Dosage =  $2.4 \times 10^{18}$  Ions/cm<sup>2</sup>
- Over 1000 min. of sputtering = CS + Dosage >  $10^{19}$  Ions/cm<sup>2</sup>

Figure 15. H<sup>-</sup> ion parallel energy distribution as a function of surface roughness for a Cs<sup>+</sup> energy of 300 eV. Hydrogen pressure is  $1.44 \times 10^{-4}$  Torr in all cases.

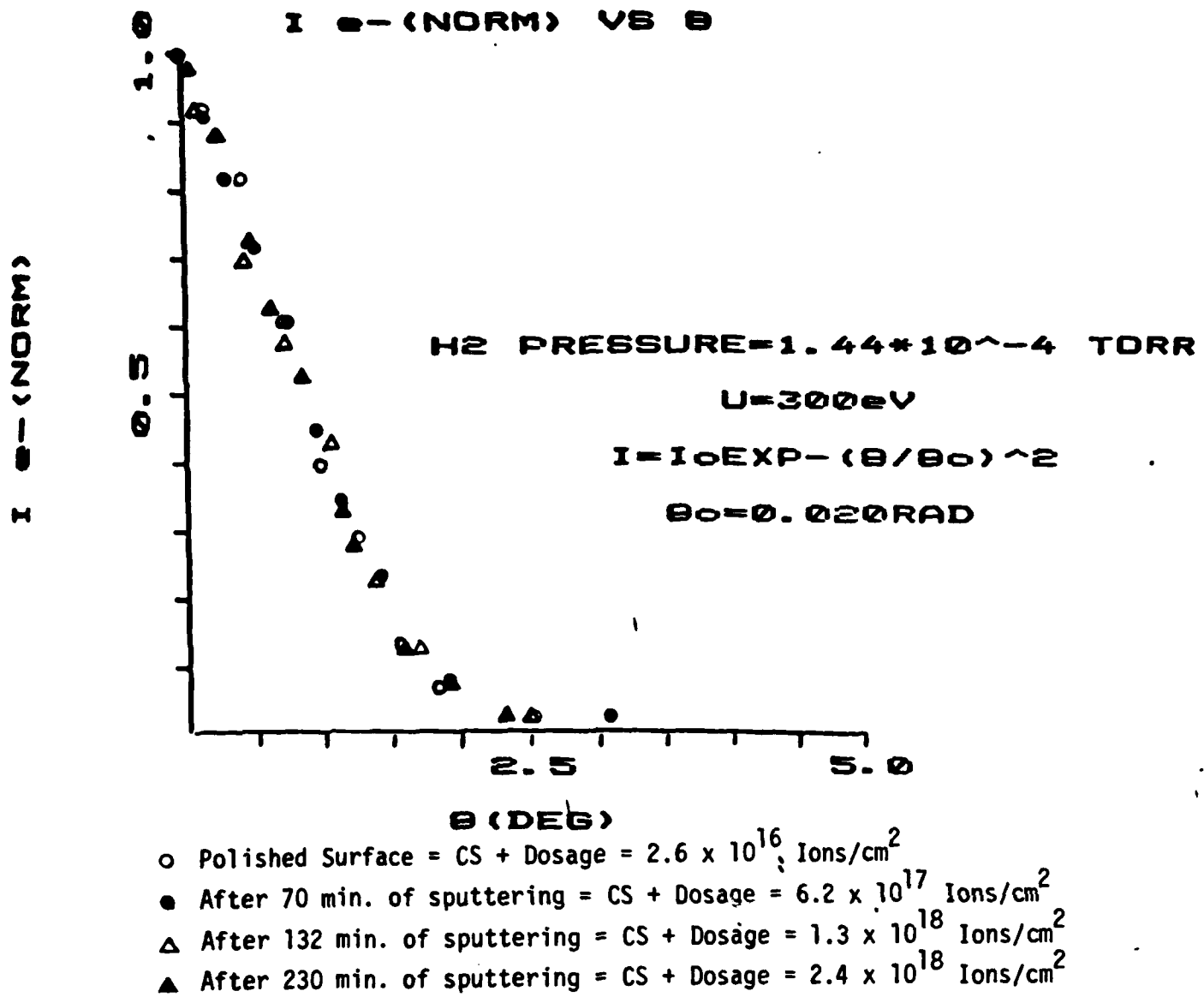
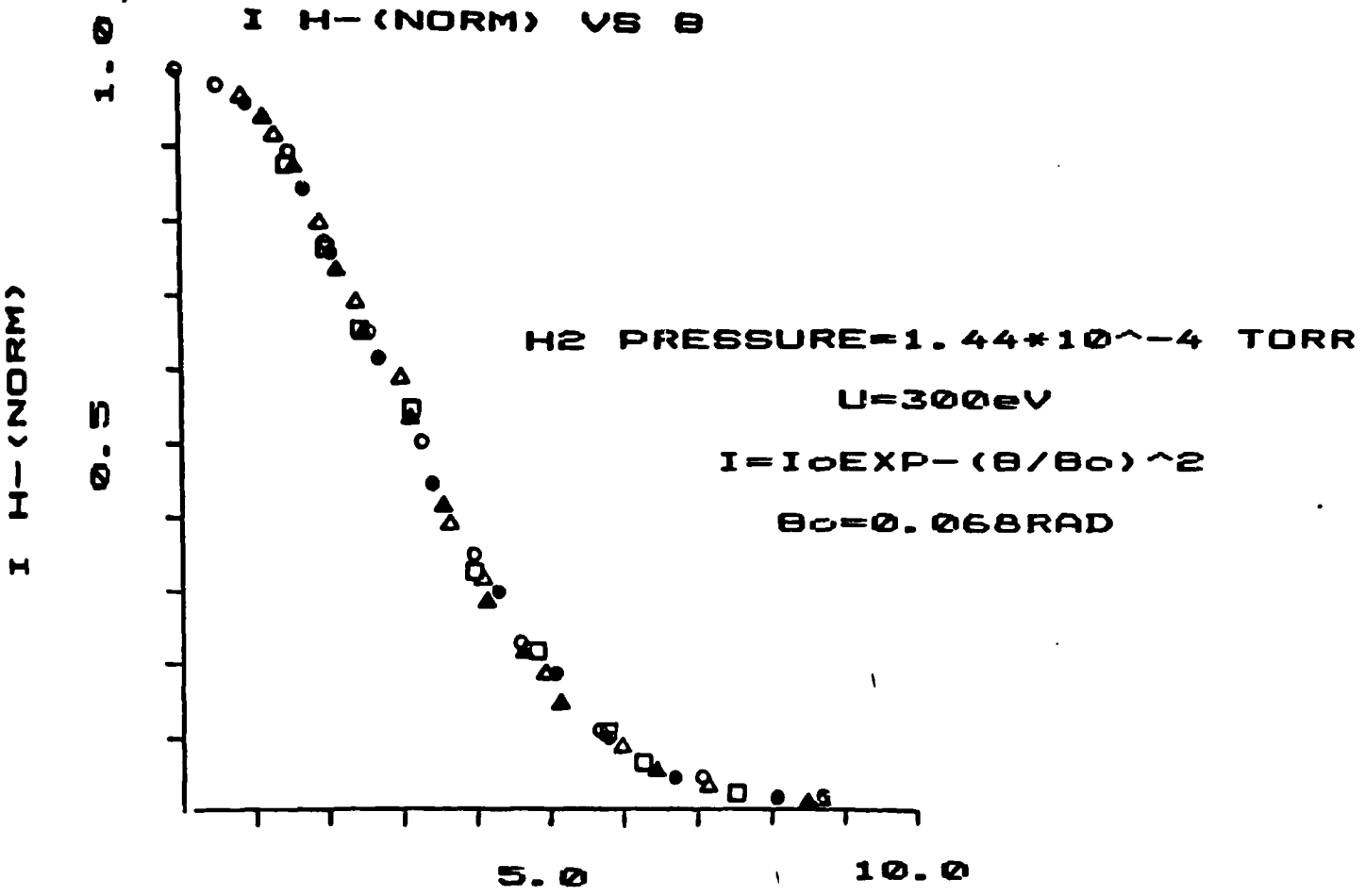


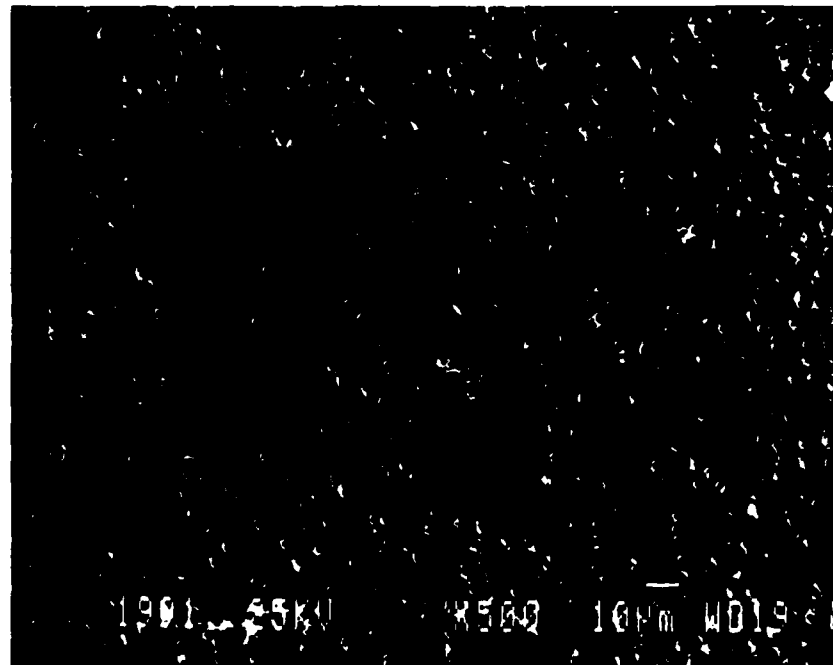
Figure 14.  $e^-$  angular distribution as a function of surface roughness for a  $Cs^+$  energy of 300 eV. Hydrogen pressure is  $1.44 \times 10^{-4}$  Torr in all cases.



- Polished Surface = CS + Dosage =  $2.6 \times 10^{16} \text{ Ions/cm}^2$
- After 70 min. of sputtering = CS + Dosage =  $6.2 \times 10^{17} \text{ Ions/cm}^2$
- △ After 132 min. of sputtering = CS + Dosage =  $1.3 \times 10^{18} \text{ Ions/cm}^2$
- ▲ After 230 min. of sputtering = CS + Dosage =  $2.4 \times 10^{18} \text{ Ions/cm}^2$
- Over 1000 min. of sputtering = CS + Dosage >  $10^{19} \text{ Ions/cm}^2$

Figure 13.  $H^-$  angular distribution as a function of surface roughness for a  $Cs^+$  energy of 300 eV. Hydrogen pressure is  $1.44 \times 10^{-4}$  Torr in all cases.

Mo Granda 2  
9-28-84



Catelog Grant

Figure 12. SEM picture of a sputtered Mo surface magnified 500 times. The target was sputtered with a  $\text{Cs}^+$  dosage of approximately  $10^{19}$  ions/cm<sup>2</sup>.

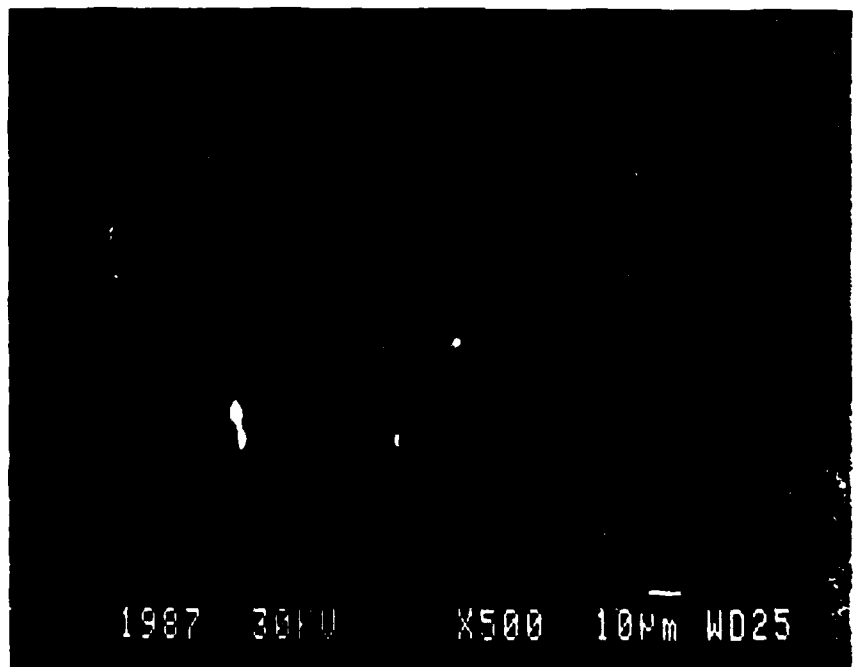
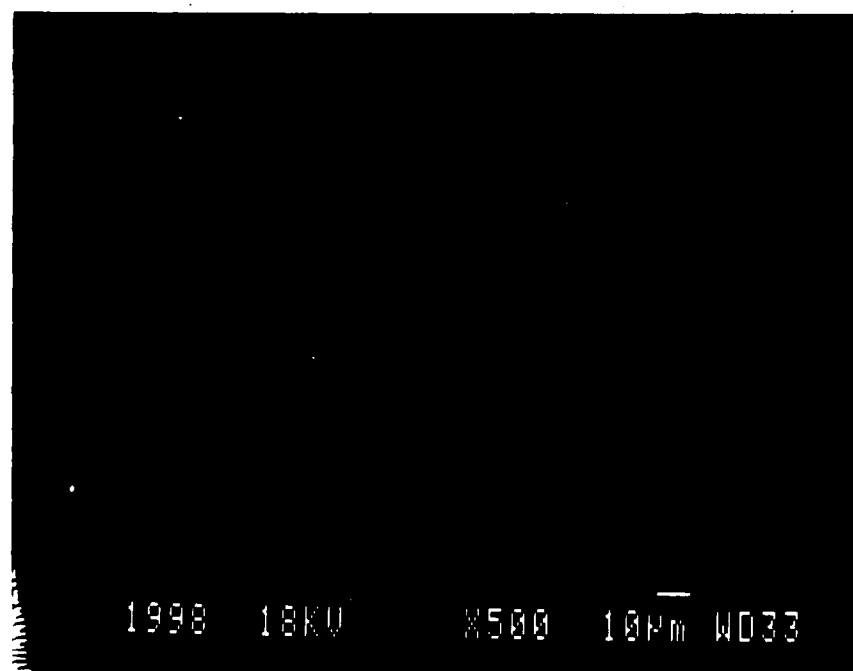


Figure 11. SEM picture of a sputtered Mo surface magnified 500 times. The target was sputtered with a  $\text{Cs}^+$  dosage of  $3.6 \times 10^{18}$  ions/cm $^2$ .



**Figure 10.** SEM picture of a polished Mo sputtering surface magnified 500 times.

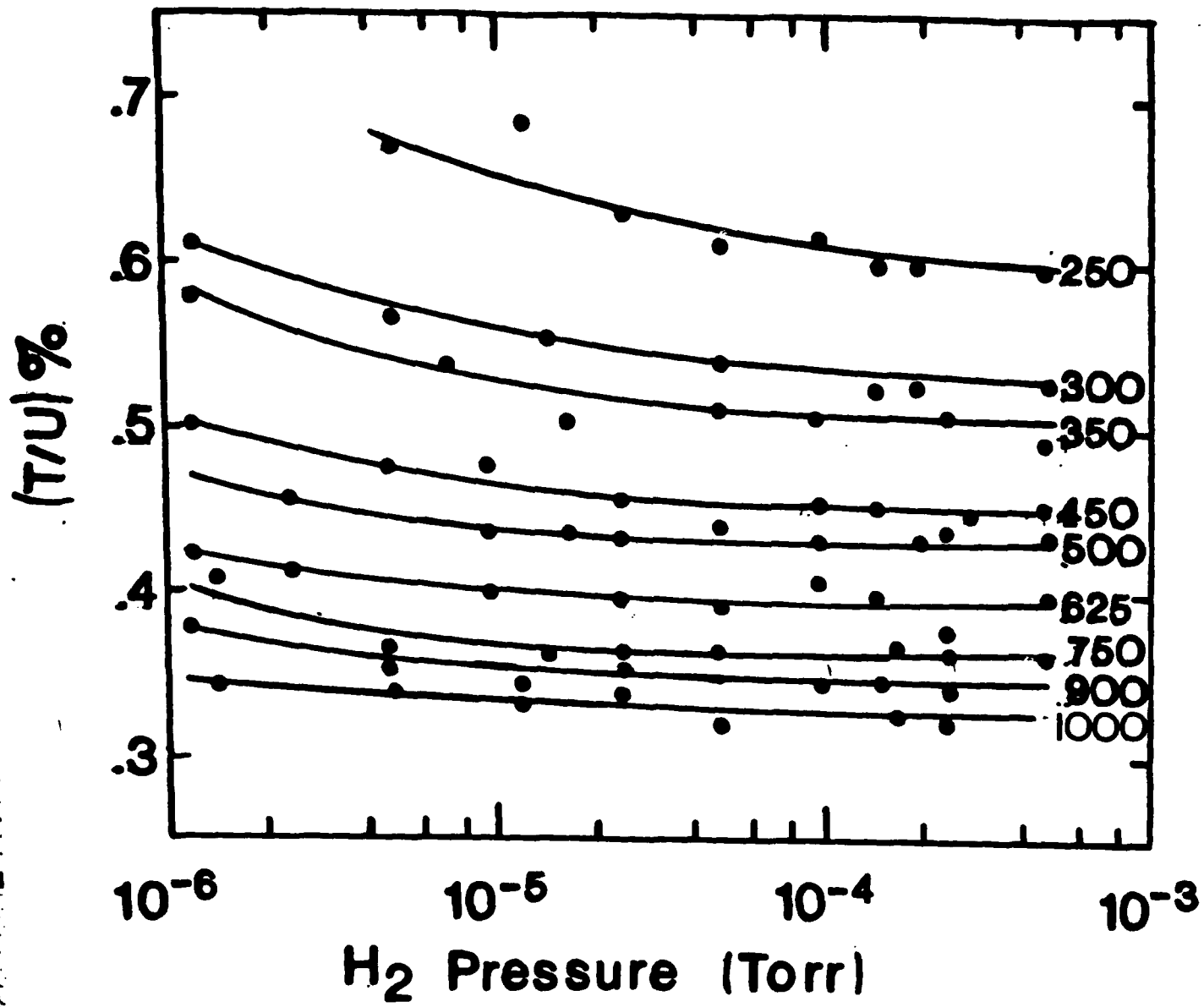


Figure 9. The  $H^+$  ion temperature as function of hydrogen pressure and  $Cs^+$  ion energy for optimum cathode workfunction.

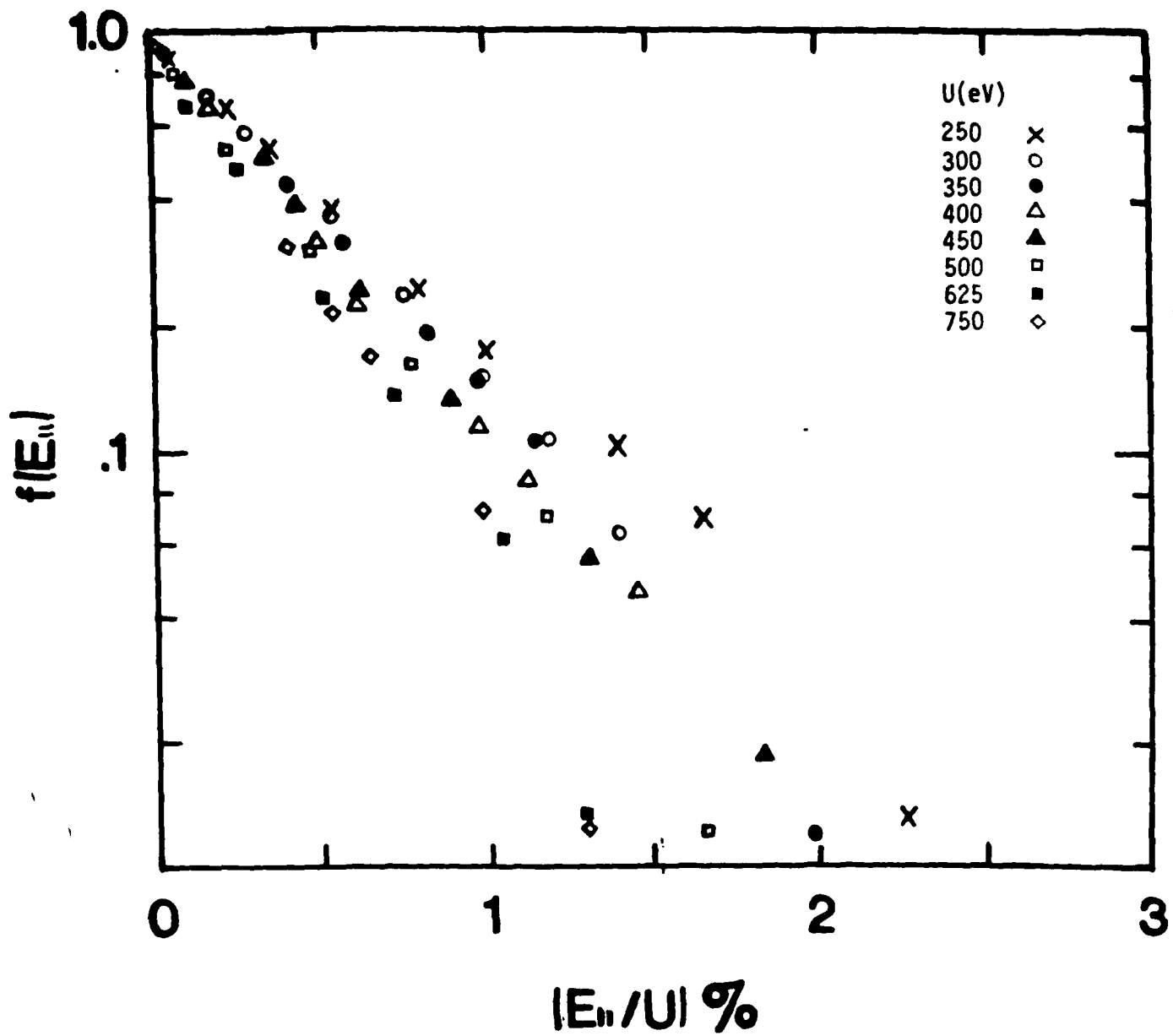


Figure 8.  $H^-$  ion parallel energy distribution for various  $Cs^+$  ion energies for optimum workfunction. The abscissa is the  $H^-$  ion energy divided by the  $Cs^+$  ion energy. Hydrogen pressure is  $2.4 \times 10^{-4}$  Torr in all cases.

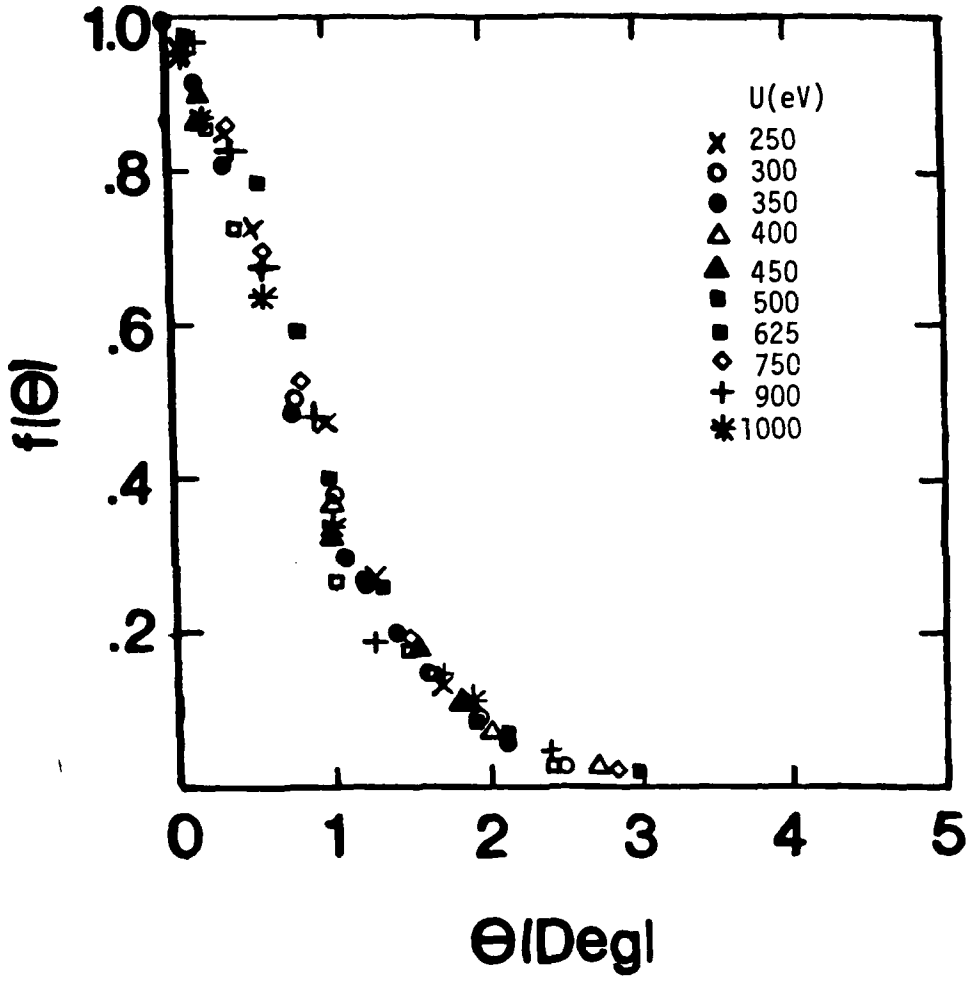


Figure 7.  $e^-$  ion angular distributions for various  $Cs^+$  ion energies for optimum cathode workfunction. Hydrogen pressure is  $2.4 \times 10^{-4}$  Torr in all cases.

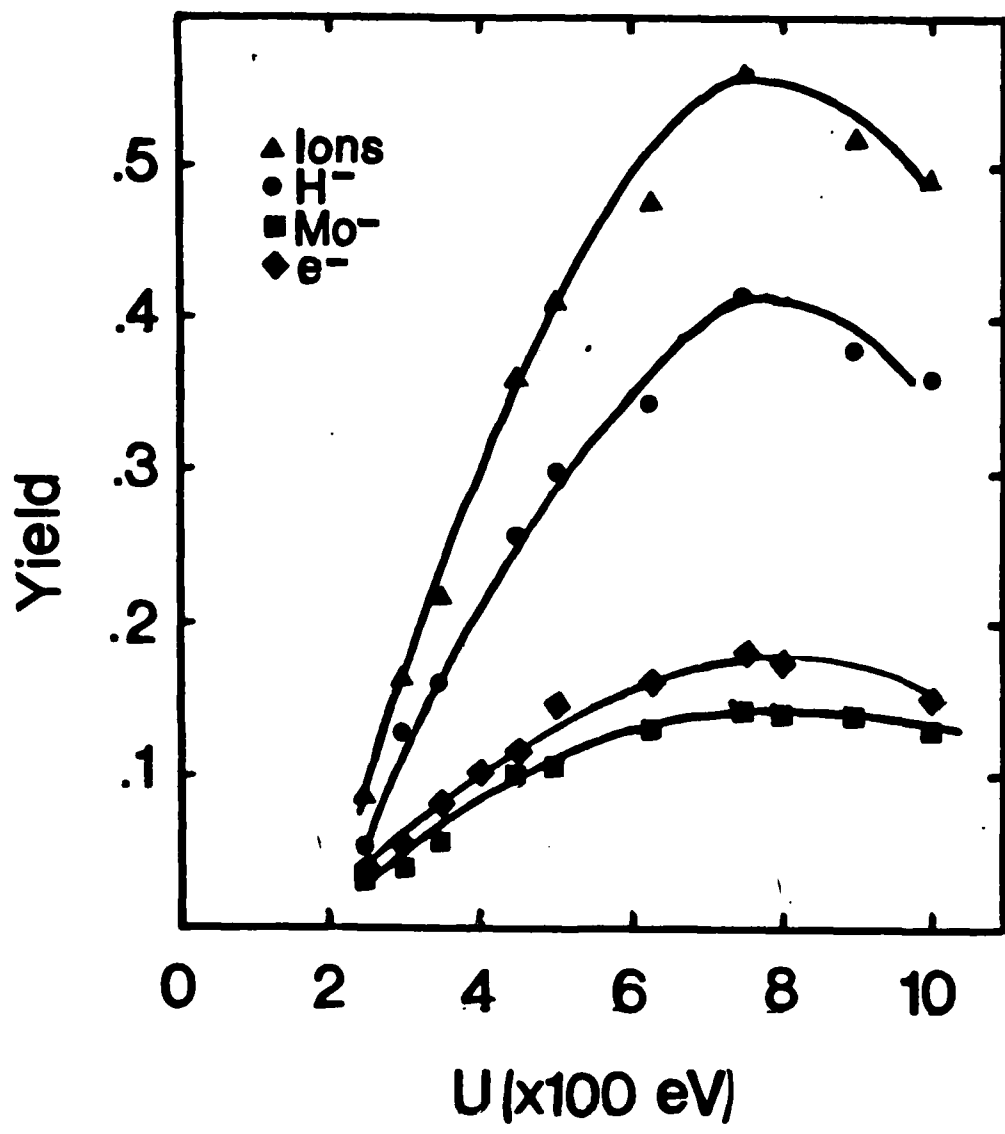


Figure 21. Optimum total ion,  $H^-$ ,  $Mo^-$ , and  $e^-$  yield as function of  $r_s^+$  ion energy.

**END**

**FILMED**

**11-85**

**DTIC**